



CSIRO
15 College Rd, Sandy Bay TAS 7005
Australia

csiro.au | ABN 41 687 119 230

3 October 2024

Our Ref: Seafloor character of the Roman Rock area in False Bay, South Africa

The Editors
EarthArXiv

Dear Editor(s)

I refer to our manuscript entitled "Seafloor character of the Roman Rock area in False Bay, South Africa" co-authored by Andrew Terhorst (Commonwealth Scientific and Industrial Research Organisation, andrew.terhorst@csiro.au) and John Rogers (University of Cape Town, johnrogers1944@gmail.com).

Note this manuscript is a non-peer-reviewed preprint submitted to EarthArXiv.

Yours truly,

A handwritten signature in black ink, appearing to read "A Terhorst", enclosed within a large, horizontal, oval-shaped scribble.

Andrew Terhorst
Senior Experimental Scientist
andrew.terhorst@csiro.au
61 400 869 594

1

2 Seafloor character of the Roman Rock area in False Bay, South Africa.

3 Andrew Terhorst^a and John Rogers^b

4 ^aCommonwealth Scientific and Industrial Research Organisation, Hobart, Australia;

5 ^bDepartment of Geology, University of Cape Town, Rondebosch, South Africa

6 **ARTICLE HISTORY**

7 Compiled October 2, 2024

8 **ABSTRACT**

9 A 12 km² area off Simon's Town in NW False Bay, South Africa, was surveyed using
10 side-scan sonar and a single-beam echosounder, revealing six distinct patterns of
11 acoustic reflectivity or acoustic facies.

12 The first facies show Cape Peninsula Granite outcrops, matching onshore patterns,
13 with lineaments reflecting the principal WNW-ESE joint direction. The second facies
14 indicate stationary, long-crested, trochoidal wave ripples, likely formed by currents
15 from southeasterly gales. The third facies shows an uneven grey tone representing
16 calcareous gravelly sand derived from marine organisms in the shallower western
17 areas. The fourth facies shows up as "Cloud-like" and "tongue-like" light patches,
18 indicating windows of underlying rippled quartzose sand. The continuous light tone
19 of the fifth facies represents a blanket of fine, rippled, quartzose sand in the deeper
20 eastern regions. The sixth facies consists of medium-grey patches within Facies 5,
21 possibly representing coarse sediment, pending further confirmation.

22 Analysis of sediment samples shows that the calcareous and quartzose sediments
23 mix according to the Folk and Ward (1957) sediment-mixing model. Quartzose
24 sands probably originate from Late Pleistocene regressive dunes reworked during
25 the Holocene transgression. Modern calcareous sediments originate from carbonate-
26 secreting organisms either attached to granite outcrops or unattached on the seafloor
27 surface. The sub-tidal environment is predominantly calm, with occasional high-
28 energy conditions due to southeasterly gales influencing sediment movement.

29 **KEYWORDS**

30 False Bay; South Africa; seafloor mapping; side-scan sonar; diver observations

31 **1. Introduction**

32 This paper revisits and updates an earlier, unpublished study (Terhorst, 1987) that
33 explored the seafloor geology around the Roman Rock lighthouse, located in the north-
34 west corner of False Bay, South Africa. The initial investigation employed side-scan
35 sonar and single-beam echosounder technologies to map the area's seafloor geology,
36 complemented by grab samples and diver inspections to validate the sonar interpreta-
37 tions. This revision summarises the foundational work and reexamines its conclusions
38 using recent geological and physical oceanographic data, providing a contemporary
39 perspective on the findings. Recognising that technological advancements can reshape
40 our methodologies, this paper argues for the enduring value of earlier techniques when
41 applied thoughtfully and supplemented with new information. We aim to bridge the

42 gap between past and present research, renewing interest in the seafloor geology of
 43 False Bay and underlining the importance of continuous exploration in marine science.

44 Numerous geological studies have been conducted in False Bay, offering a com-
 45 prehensive understanding of the region. These studies are summarised in Table 1.
 46 Research covering the entire bay includes works by Morgans (1956),Bowie (1966),Simp-
 47 son, Du Plessis and Forder (1970),Gentle (1971),Flemming (1982), and Du Plessis and
 48 Glass (1991). Other studies have focused on specific areas within False Bay: Retief’s
 49 1970 research focuses on sediment transport patterns in Gordon’s Bay (Retief, 1970),
 50 while Flemming (1976) explores the evolution of Rocky Bank at the entrance of False
 51 Bay. Erosion of the northern shoreline, particularly around Strandfontein and Mon-
 52 wabisi Beach, has been studied by Schoonees, Scholtz, Van Tonder, Moller and Lenhoff
 53 (1983), Fourie, Ansorge, Backeberg, Cawthra, MacHutchon and van Zyl (2015), and
 54 MacHutchon (2015). Van Zyl (2011) documented a side-scan sonar survey along the
 55 western shore that forms part of the Table Mountain Marine Protected Area.

56 This localised study, originally commissioned by the Institute for Maritime Technol-
 57 ogy (IMT) on behalf of the South African Navy Hydrographic Office, stands out as
 58 one of the most detailed geological explorations in False Bay to date.

59 As to the organisation of this paper, the following section describes the physical
 60 setting of False Bay. This description covers (a) the physiography of the bay, (b) its
 61 seafloor geology, and (c) various aspects of the bay’s physical oceanography. The paper
 62 then explains how the data in the Roman Rock area were collected and processed,
 63 followed by a presentation and discussion of the results of the data analysis. It concludes
 64 with a summary of the main findings and recommendations for further research.

Table 1.: Other geological studies undertaken in False Bay.

Source	Description of research
Murray and Renard (1891)	Describe a single sediment sample collected off Simon’s Town in their report on marine sediment samples collected during the 1873 to 1876 “Challenger” expedition.
Morgans (1956)	Analyse the relationship between sediment type and benthic fauna in False Bay.
Fuller (1961, 1962)	Analyse the textural properties of sediment samples collected from nearshore and beach environments around False Bay.
Bowie (1966)	First geological study of the entire False Bay.
Bowie, Fuller and Siesser (1970)	Describe the sediments in False Bay.
Mallory (1970)	Describe the bathymetry and microrelief of False Bay.
Retief (1970)	Report on sediment transport patterns in Gordon’s Bay.
Simpson et al. (1970)	Report on a bathymetric and magnetic survey conducted to the west of the Cape Peninsula and in False Bay.
Gentle (1971, 1973)	Interpret the seafloor geology from a side-scan sonar traverse across False Bay.
Flemming (1976)	Describes Rocky Bank as a relict wave-cut terrace.
Glass and Du Plessis (1976)	Describe the bathymetry of False Bay in relation to its geology.
Glass (1977)	Describes deep weathering in the Cape Peninsula Granite beneath the False Bay seafloor.
Marchant and Flemming (1978)	Discuss the significance of granite erratics in a sandstone boulder beach along the western shore of False Bay.
Glass and Gasson (1980)	Present an overview of the geology of False Bay.
Russell-Cargill (1982)	Compiles a side-scan sonar mosaic of a small part of Simon’s Bay.
Flemming (1982)	Report on the geology of False Bay with particular emphasis on its modern sediments.
Schoonees et al. (1983)	Study of sediment dynamics off Strandfontein.
Day (1986)	Mapped dolerite dykes beneath the False Bay seafloor from magnetic data.
Du Plessis and Glass (1991)	Presents a detailed description of the geology of False Bay
Theron and Schoonees (2007)	Describe sediment transport patterns off Monwabisi Beach, northern False Bay.
Backeberg, Reid, Trumbull and Romer (2011)	Describe the petrogenesis of the dolerite dykes beneath the False Bay seafloor.
MacHutchon (2015)	Mapped the seabed off Monwabisi Beach, northern False Bay.
Fourie et al. (2015)	Describe the influence of wave action on coastal erosion along Monwabisi Beach.

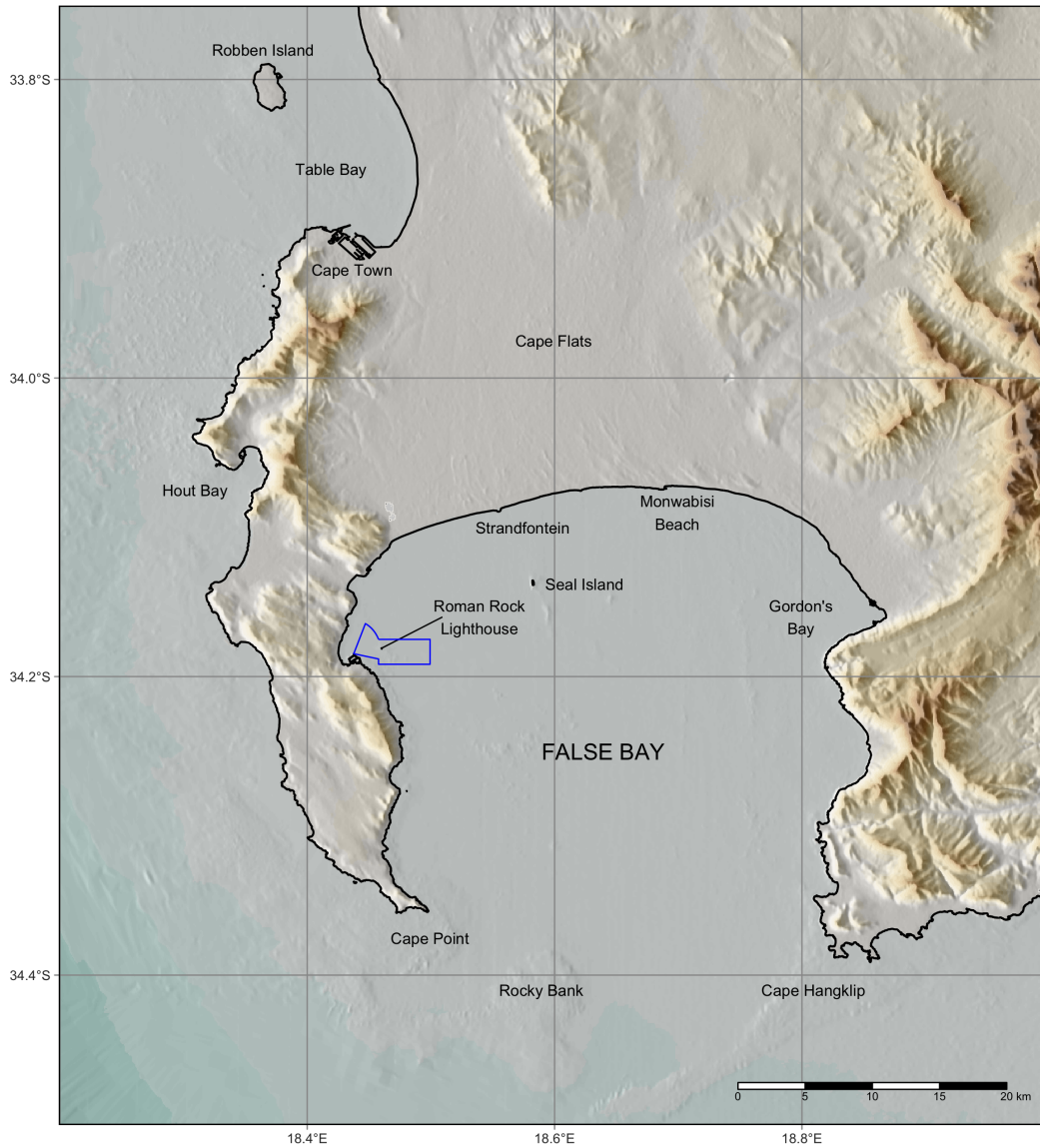


Figure 1.: Shaded relief map showing the location of the study area (outlined in blue) off Simon's Town in the NW corner of False Bay. Note the steep mountains to the west and north of the survey area that significantly influence the wind regime across False Bay. Rocky Bank focuses the energy of long-period swells entering the bay.

65 2. Physical setting

66 False Bay is the southward extension of a broad sandy valley known as the “Cape Flats”
67 situated between the mountainous Cape Peninsula to the west and the Hottentots-
68 Holland Mountains to the east (Figure 1). The seafloor within the bay slopes at a
69 gradient of 1:370 toward the south, reaching a depth of over 100m between Cape Point
70 and Cape Hangklip (Du Plessis and Glass, 1991; Glass and Du Plessis, 1976; Rogers,
71 2018). Apart from rock pinnacles and reefs around Roman Rock, Seal Island, York
72 Shoal, East Shoal, and Whittle Rock, the seafloor in the western and southern parts
73 of the Bay is relatively smooth, unlike the seafloor in the eastern part, which is more
74 irregular (Du Plessis and Glass, 1991). Rocky Bank at the entrance to False Bay affects
75 how ocean swells enter the Bay.

76 2.1. Geology

77 The geology of False Bay is inferred from onshore geological maps, hand-contoured
78 hydrographic survey fair-charts, dredge and grab samples, and from magnetometer,
79 shallow seismic and side-scan sonar traverses (Du Plessis and Glass, 1991).

80 2.1.1. Bedrock geology

81 Cambrian (~ 540 my) Cape Peninsula Granite underlies the western half of False
82 Bay. The Cape Peninsula Granite intruded the Cambrian (~ 560 my) Malmesbury
83 Supergroup shale that underlies the eastern half of False Bay (Belcher and Kisters,
84 2003; Scheepers and Schoch, 2006). The Ordovician Table Mountain Group’s erosion-
85 resistant sandstone overlies the Cape Peninsula Granite and Malmesbury Supergroup.
86 The sandstone forms the mountainous terrain flanking the western and eastern sides of
87 False Bay (Theron, 1984).

88 The granite outcrops along the coast south of Simon’s Town tend to be blocky and
89 well-jointed with deep weathering in places (Rogers, 2018, p. 253 – 274). Seismic profiles
90 show that False Bay’s granite is deeply weathered in places. Joint spacing probably
91 controls the depth of weathering – the closer the spacing, the deeper the weathering
92 (Linton, 1955). Granite outcrops are more likely to occur where joints are more widely
93 spaced (Glass, 1977).

94 Roman Rock lighthouse, situated in the middle of the study area, is built on top of
95 a large granite tor that protrudes above the sea surface (Figure 2). South of Simon’s
96 Town, the unconformity between the Cape Peninsula Granite and the Table Mountain
97 Group is about 100m above the current sea level (viz. Rogers (2018, p.64)). The
98 unconformity dips below sea level north of Simon’s Town, suggesting the bedrock in
99 the northwestern corner of the study area is likely to be part of the Table Mountain
100 Group.

101 The Cape Peninsula Granite and lower parts of the Table Mountain Group have
102 been intruded by a swarm of dolerite dykes (Haughton, 1933). The dyke swarm dates
103 to the Early Cretaceous and is thought to be associated with the opening of the South
104 Atlantic (Backeberg et al., 2011). Magnetometer data indicate the presence of a large
105 WNW-ESE trending dolerite dyke in the Cape Peninsula Granite beneath the study
106 area (Simpson et al., 1970).



Figure 2.: Roman Rock lighthouse – December 2022. The cast-iron lighthouse was built in 1861 on top of a granite tor that protrudes above the sea surface at low tide. Note the north-facing solar panels that power the lighthouse. Simon’s Town appears in the background at the base of the 678m high Swartberg mountain. Image credit: Andrew Morson.

107 *2.1.2. Unconsolidated sediments*

108 Much of the seafloor in the western half of False Bay is covered by sediment, unlike the
109 seafloor in the eastern half of the bay, which is mostly exposed Tygerberg Formation
110 siltstone (Du Plessis and Glass, 1991). Seismic profiles indicate that the thickness of
111 the unconsolidated sediment exceeds 10m in the middle of False Bay. However, it is
112 less than 2m thick in the study area (Du Plessis and Glass, 1991). Flemming (1982)
113 analysed 190 sediment samples collected in False Bay by Bowie (1966) and Glass and
114 Gasson (1980). Four of these samples were collected within the study area and show the
115 unconsolidated sediment is mostly fine to medium sand, except around granite outcrops,
116 composed of coarse bioclastic material. According to Flemming (1982), bottom-traction
117 is the primary sediment movement mechanism in the study area's western part. In the
118 deeper eastern part of the study area, the primary mechanism for sediment movement
119 is lower-bottom suspension.

120 *2.2. Physical oceanography*

121 *2.2.1. Wind regime*

122 Weather patterns at the SW tip of Africa are influenced by the interaction between
123 the South Atlantic Anticyclone (SAA), situated in the subtropical high-pressure belt,
124 and westerly (Rossby) waves in the circumpolar low-pressure belt (Schulze, 1965). The
125 position of the SAA oscillates between a southern hemisphere summer mean of 32°S
126 and a winter mean of 28°S. False Bay, at about 34°S, is dominated by anticyclonic
127 conditions in summer, and by cyclonic conditions in winter (Jury, 2020). Consequently,
128 the physical oceanography of False Bay is dominated by a bidirectional wind regime,
129 with winds blowing seasonally from opposing quarters. Figure 3 depicts the monthly
130 wind speed distribution and wind direction near Simon's Town. It is based on ERA5
131 monthly averaged data on single levels from 1979 to the present (Hersbach, Bell,
132 Berrisford, Hirahara, Horányi, Muñoz-Sabater, Nicolas, Peubey, Radu, Schepers et al.,
133 2020). Simon's Town area is dominated by SE winds from October to April and by
134 NW winds from May to September. SE winds tend to blow harder than the NW winds.

135 The mountainous terrain of the Cape Peninsula strongly influences wind patterns
136 in the study area (Jury, 2020). As Figure 1 shows, mountains shield the study area
137 from strong NW winds. However, the same mountains also channel strong SE winds
138 (Coleman, Diedericks, Theron and Lencart e Silva, 2021). Gale-force SE winds can
139 generate rough seas across the study area.

140 *2.3. Thermal structure*

141 Atkins (1970a) was the first to analyse the thermal structure of False Bay. His data
142 show that sea-surface temperatures (SSTs) in the study area range from 20.3 °C in
143 summer to 14.8 °C in winter. Bottom temperatures in the study area range between
144 12.2 °C in summer to 14.3 °C in winter. Recent circulation models support earlier
145 conclusions that the pronounced thermocline observed in summer is caused by SE
146 winds pushing warmer surface water into the bay (Coleman et al., 2021; Grundlingh
147 and Potgieter, 1993; Wainman, Polito and Nelson, 1987).

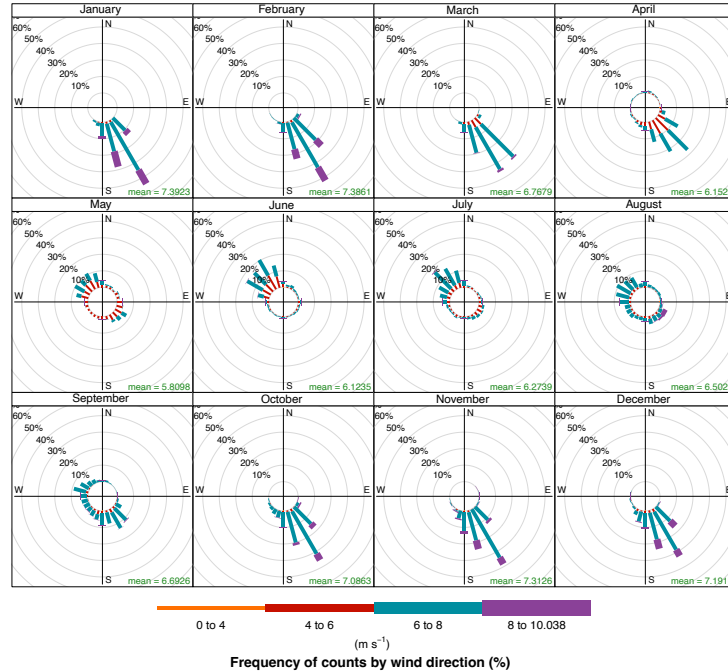


Figure 3.: ERA5 monthly average wind speed and direction in False Bay (34.25S, 18.5E). ERA5 is the fifth generation European Centre for Medium-Range Weather Forecasts (ECMWF) reanalysis for global climate and weather.

148 *2.4. Tidal regime*

149 Analysis of historical tide-gauge data shows that Simon’s Town experiences a spring-
 150 tide range of 1.486 meters. False Bay falls into a semi-diurnal upper micro-tidal (≈ 2 m
 151 tidal-range) environment (Davies, 1980; Grundlingh and Largier, 1991; Stephenson,
 152 2016). With such a regime, tidal currents are expected to be relatively weak in the
 153 study area (Rautenbach, Barnes and de Vos, 2019; Vos, Vichi and Rautenbach, 2021).
 154 Data from an Acoustic Doppler Current Profiler (ADCP) deployed off Miller’s Point,
 155 6km south of Simon’s Town, show that tide-driven bottom currents never exceed 0.1
 156 ms^{-1} (Coleman et al., 2021).

157 *2.5. Swell regime*

158 Southwesterly swells dominate the southwest coast of South Africa. The Cape Peninsula
 159 provides a natural barrier protecting much of False Bay from the direct impact of these
 160 swells. Rocky Bank, at the mouth of False Bay, focuses the energy of southwesterly
 161 swells on the rocky eastern shoreline of False Bay, as detailed in studies by Shipley
 162 (1964), Darbyshire (1966), and more recently by Salonen and Rautenbach (2021). This
 163 phenomenon poses significant risks, especially to anglers along the eastern shore, some
 164 of whom have been swept off the rocky coastline by massive waves.

165 Southerly swells, originating from deep low-pressure systems south of the country,
 166 occasionally penetrate the bay. These swells, too, are concentrated by Rocky Bank, but
 167 their impact is felt predominantly along the northwest shore of False Bay. This concen-
 168 tration of energy can cause considerable damage to coastal structures, as documented

169 by MacHutchon (2015) and Pfaff, Logston, Raemaekers, Hermes, Blamey, Cawthra,
170 Colenbrander, Crawford, Day, Du Plessis et al. (2019). The eastern half of our study
171 area lies directly in the path of these focused swells, a phenomenon illustrated in Figure
172 4.

173 Data from the above-mentioned ADCP show that wave heights in the northwest
174 corner of False Bay can reach 1.5m (Daniels, Fearon, Vilaplana, Hewitson and Raut-
175 enbach, 2022). However, such wave heights tend to be associated with shorter-period
176 waves between 4s and 6s, typically generated by strong local winds.

177 *2.6. Surface and bottom currents*

178 Atkins (1970b) found wind-driven surface currents dominate False Bay. He describes a
179 clockwise circulation driven by SE winds and an anti-clockwise circulation driven by
180 NW winds. Current meters show that surface water is driven into the middle of the
181 bay by SE winds and exits on the eastern and western sides (Grundlingh and Largier,
182 1991; Wainman et al., 1987).

183 Circulation models indicate complicated surface-current patterns for different wind
184 speeds and wind directions (Jury, 2020; Vos et al., 2021). Bottom currents tend to flow
185 differently from surface currents (Coleman et al., 2021; Vos et al., 2021). The models
186 show that in the study area, surface and bottom currents move in a northerly direction
187 with SE winds. With NW winds, surface currents move in a southerly direction. In
188 contrast, bottom currents move in the opposite direction (Coleman et al., 2021). In
189 other words, wind-driven bottom currents flow northwards through the study area, no
190 matter how the wind blows. Tide-driven currents develop when there is no wind-forcing
191 and flow northward during incoming tides and southward during outgoing tides (Vos
192 et al., 2021).

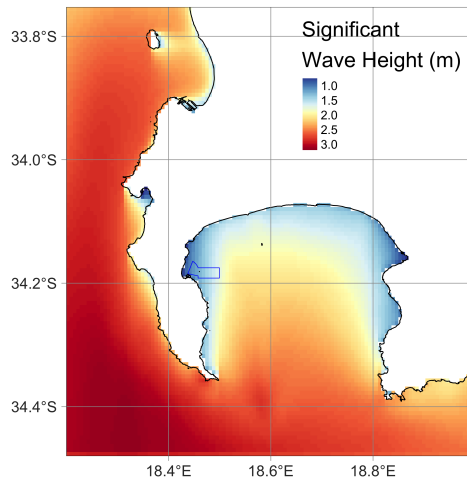
193 **3. Methods**

194 *3.1. Data collection*

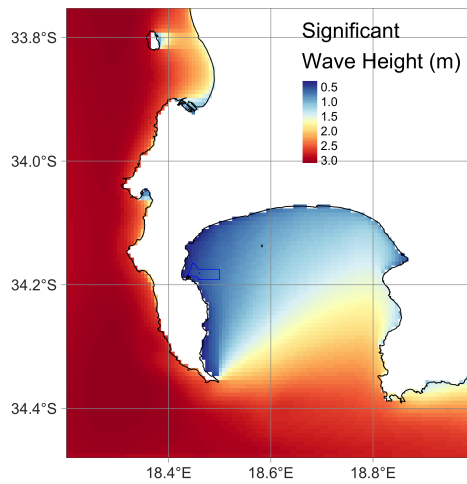
195 Data collection occurred in two stages during 1985 and 1986. The initial phase involved
196 seafloor mapping using side-scan sonar and echosounder, followed by sediment sampling
197 and diver inspections for verification in the second phase. This was conducted using two
198 catamaran workboats, the Shirley-T and Annie-K (Figure 5), equipped for surveying
199 and diving.

200 *3.1.1. Geophysical survey*

201 An integrated survey system, comprising an autopilot, single-beam echosounder, and an
202 analogue side-scan sonar system, steered a small catamaran boat along predetermined
203 tracks. A microwave ranging system provided one-meter accuracy position fixes (the
204 survey was conducted before GPS became prevalent). The survey unfolded in two
205 phases: The first phase recorded 7811 depth soundings at one-second intervals along 66
206 east-west tracks spaced 60m apart (Figure 6). The second phase collected 10.8km² of
207 100kHz side-scan sonar imagery along 22 east-west tracks spaced 180m apart (Figure
208 11). Tracks were traversed at 3.5 knots to achieve a 2m along-track resolution. The
209 system produced side-scan sonar imagery, corrected for speed and slant range, at a
210 1:1000 scale, with position fixes marked every 30 seconds on the paper records.



(a) Southerly swell - 2008-08-30 14:00



(b) Southwesterly swell - 2009-09-09 18:00

Figure 4.: Modelled wave heights in False Bay illustrating the shielding effect of the Cape Peninsula on swell encroachment in False Bay. The focusing effect of Rocky Bank is apparent in the southerly swell scenario. SWAN model outputs courtesy of Christo Rautenbach and Marc de Vos.



(a) Shirley-T



(b) Annie-K

Figure 5.: Catamaran workboats used for data collection

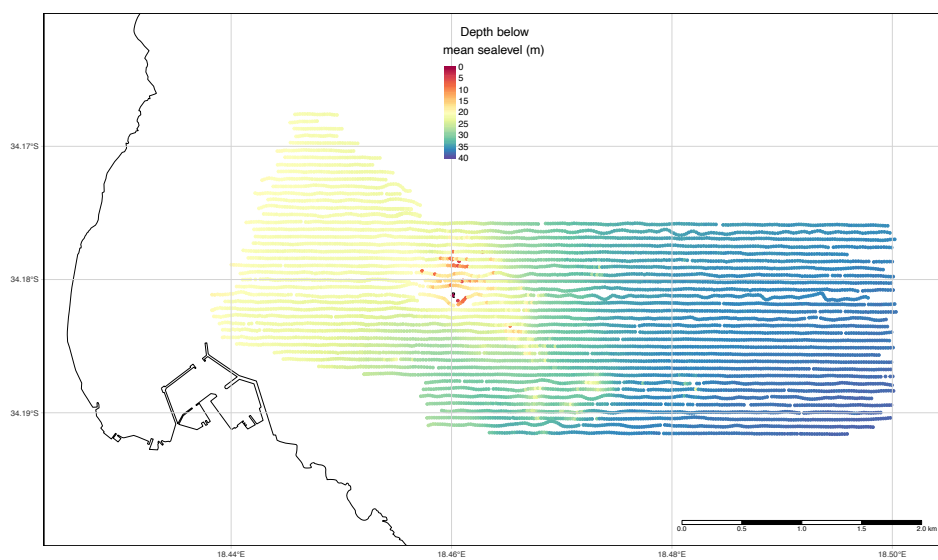


Figure 6.: Depth soundings along 66 east-west oriented survey tracks

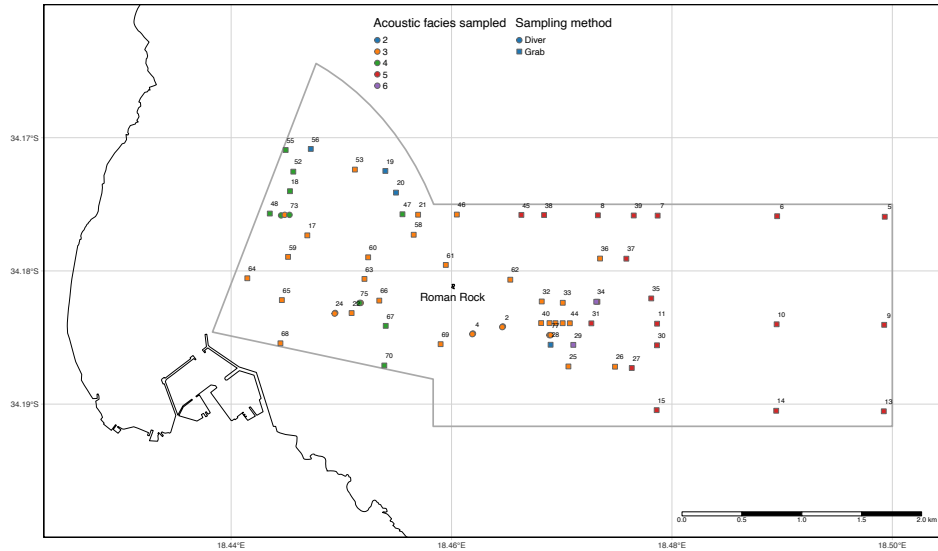


Figure 7.: Sediment sample sites. Colors indicate which acoustic facies were sampled. Shapes indicate the sampling method used.

211 3.1.2. Sediments sampling and diver-inspections

212 Proper interpretation of side-scan sonar imagery requires quality ground control (Bouma
 213 and Rappeport, 1984). To avoid misinterpretation of the side-scan sonar imagery,
 214 sediment samples and information from SCUBA diver inspections were obtained from
 215 several locations within the study area.

216 This study collected 71 sediment samples: 66 were obtained using a hand-operated
 217 Van Veen grab (Lie and Pamatmat, 1965), and SCUBA divers collected five during
 218 seafloor inspections. The sampling sites targeted different patterns of acoustic reflectivity
 219 (acoustic facies) observed on the side-scan sonar imagery. Figure 7 shows the location
 220 of each sample site. The Van Veen grab retrieved up to 0.6 liters of sediment. Retrieved
 221 samples were emptied into a bucket to allow fines to settle and remove macrofauna
 222 and excess water, before being transferred into a labeled 700ml jar. Diver-collected
 223 samples were scooped into similar jars and capped underwater before being brought to
 224 the surface.

225 The SCUBA divers inspected different patterns of acoustic reflectivity at ten dive
 226 sites (Figure 8). Ten divers, including three marine geologists and one marine biologist,
 227 participated. For safety, dives were limited to fair weather and depths under 30m,
 228 restricting sites to the study area's shallower western part. Sediment samples were
 229 collected at six dive sites. Divers recorded notes on plastic sheets and took underwater
 230 photographs using 200 ISO color slide film using a Nikonos IV A camera.

231 3.2. Data processing and analysis

232 3.2.1. Geophysical survey

233 The 1:1,000 scale paper imagery was reduced to 1:2,000 scale using a photocopier for
 234 easier handling. These reduced copies were arranged in a mosaic on a lab floor, allowing
 235 the first author to identify various sonograph facies based on acoustic reflectivity, as

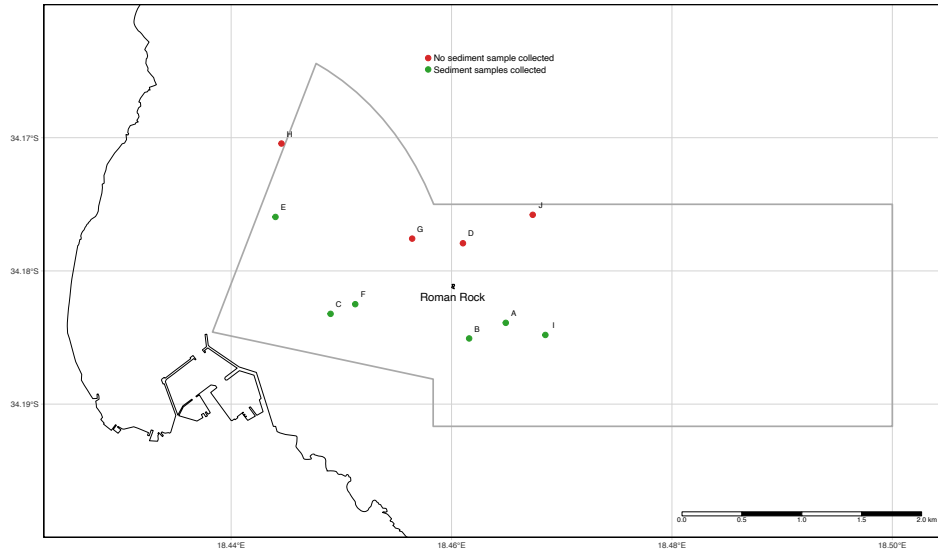


Figure 8.: SCUBA dive sites. All the dive sites are in water less than 30m deep. Sediment samples were collected at six of the dive sites.

236 outlined by (Kidd, Simm and Searle, 1985). Underwater Surveys then transferred these
 237 facies onto 1:2,000 scale track charts, which were photographically reduced to 1:10,000
 238 scale and compiled into a single map. This map was digitised as an ESRI shapefile for
 239 integration with other spatial data.

240 The 7811 depth soundings, time-stamped and tide-corrected, were converted into
 241 XYZ data points. One-meter interval depth contours were generated from these data
 242 using TNTmips software and saved as an ESRI shapefile.

243 *3.3. Sediment sample analysis*

244 The workflow used to determine the textural and compositional properties of all the
 245 sediment samples is presented in Figure 9.

246 *3.3.1. Sample preparation*

247 The wet sample was split by coning and quartering, and a quarter was put aside for
 248 laboratory analysis. The laboratory sub-sample underwent desalination via osmosis in
 249 dialysis tubing immersed in refreshed tap water overnight. This desalinated sample
 250 was then split again, allocating three-quarters for texture analysis and the remaining
 251 quarter for composition analysis.

252 *3.3.2. Sieving*

253 The desalinated texture split was wet-sieved through a $63\mu\text{m}$ screen, separating the mud
 254 (less than $63\mu\text{m}$) from the coarser fraction. The mud was allowed to settle in plastic
 255 tubs, decanted, and then dried in glass beakers at 100°C for 24 hours for weighing.
 256 The coarse fraction underwent similar drying, followed by a 5-minute mechanical sieve
 257 through $63\mu\text{m}$ and 2mm screens to separate gravel, sand, and pan-mud – the latter
 258 being silt retained on the $63\mu\text{m}$ screen due to water surface tension. After weighing,

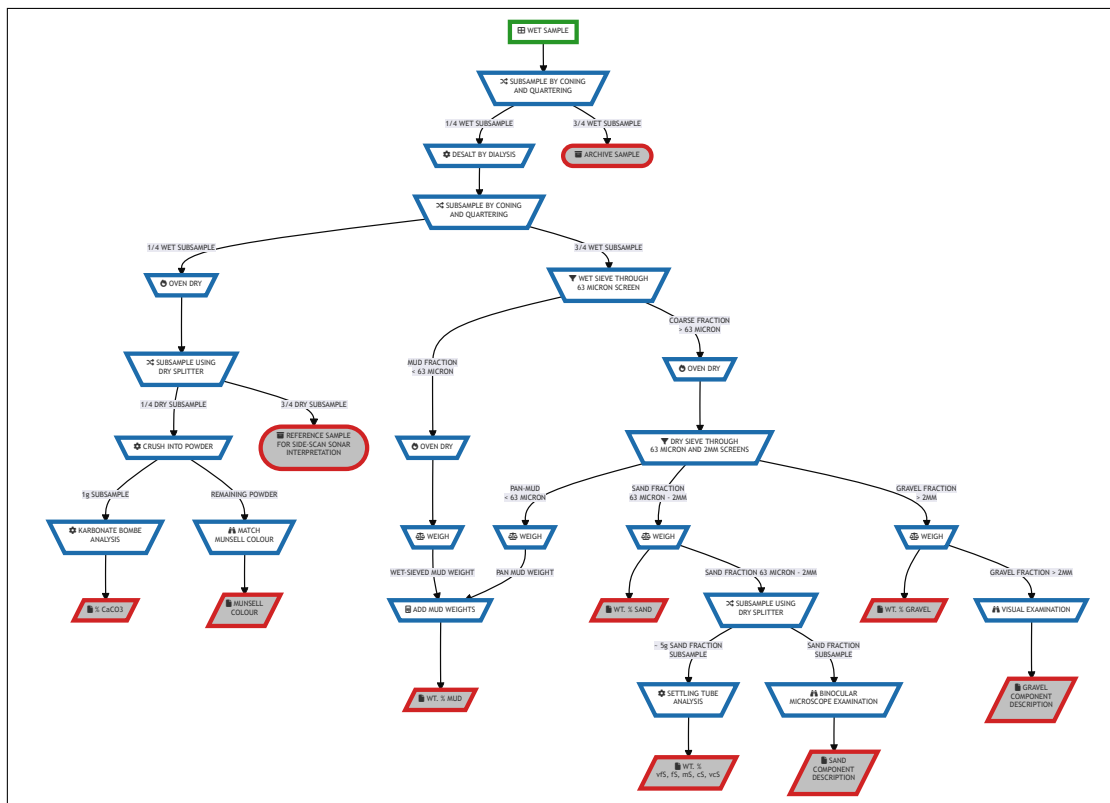


Figure 9.: Sediment sample analysis workflow

259 pan-mud was added to the wet-sieved mud weight for total mud weight calculation.
260 The gravel, sand, and mud proportions were then calculated as percentages of the total
261 dry weight.

262 *3.3.3. Sand size-analysis*

263 For settling-tube analysis, less than 10g of the sand fraction was sub-sampled using
264 a dry sample splitter. Equipment issues meant samples had to be analysed using the
265 Council for Geoscience and the University of Cape Town settling tubes. These shared
266 the same basic hardware configuration and microcomputer setup – the software for
267 performing rapid and precise statistical analysis of sand-size distribution was essentially
268 identical (Brink and Rogers, 1985; Flemming and Thum, 1978).

269 *3.3.4. Calcium carbonate analysis*

270 The desalinated composition-split was oven-dried and then split again. One quarter was
271 crushed into a fine powder with the remaining three-quarters used as a reference sample
272 for the sonograph interpretation. Each crushed sub-sample was colour-coded using
273 Munsell (1975) soil-color charts before being analyzed for CaCO₃ using the “Karbonat
274 Bombe” method (Birch, 1981; Müller and Gastner, 1971).

275 Five millilitres of concentrated hydrochloric acid (HCl) was added to 1g of the
276 crushed sample in an airtight container fitted with a pressure gauge. The pressure
277 of the released gas was normalised against a standard for pure CaCO₃, giving the
278 percentage CaCO₃ for the sample. Standards were determined every five samples as
279 this method is sensitive to air temperature and atmospheric pressure variations.

280 *3.4. Megascopic description of components*

281 The gravel and sand fraction components were examined using a procedure based
282 on the Ingram (1965) method. The gravel fraction was inspected visually, while the
283 sand fraction was examined under a binocular microscope. Each sample’s components
284 were identified, and their relative abundances were categorised as ‘dominant’ (>50%),
285 ‘major’ (5-50%), ‘minor’ (1-5%), or ‘trace’ (> 1%). Identification of specific biogenic
286 components required consultation with marine biologists.

287 **4. Observations**

288 *4.1. Bathymetry*

289 An NW-SE oriented reef divides the study area into two, as shown in Figure 10. This
290 reef, around two kilometres long and one kilometre wide, features several steep granite
291 pinnacles rising 2 to 20 meters above a smooth seafloor. Notably, three pinnacles pose
292 navigational hazards: Roman Rock, marked by a lighthouse; Castor Rock, shallowest
293 at about three meters; and Rambler Rock, with a minimum depth of eight meters. To
294 the northwest, the seafloor is flat and 20-22 meters deep, whereas to the southeast, it
295 forms a narrow trough, less than a kilometre wide and up to 33 meters deep, between
296 the reef and coast. East of the reef, the seafloor gradually deepens from 25m to 38m
297 towards the southeast corner of the area, with a slight channel-like depression observed
298 northwest of Roman Rock.

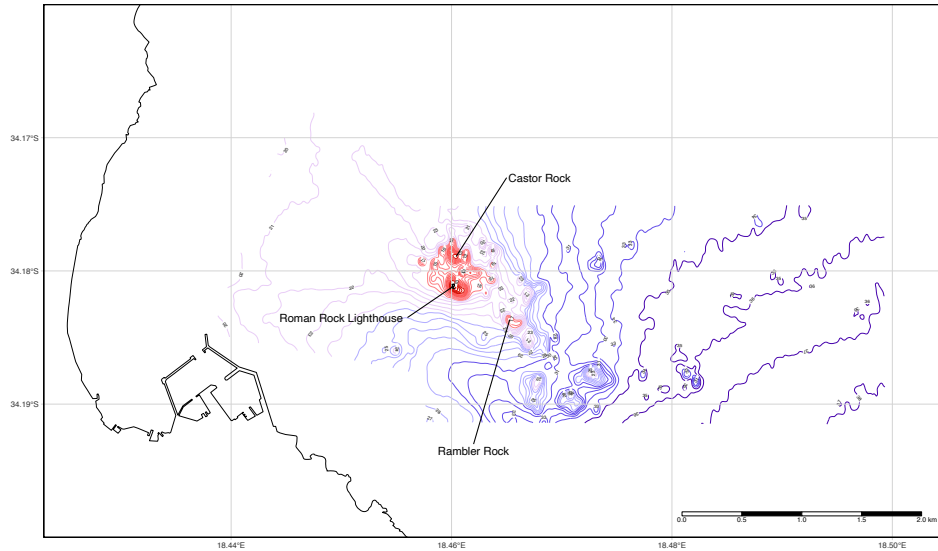


Figure 10.: Bathymetry of the study area (one-meter contour-interval).

299 **4.2. Side-scan sonar survey**

300 Equipment issues and the need to navigate around shallow and exposed reefs meant
 301 that only 90% of the study area was surveyed by side-scan sonar (10.8 km²). Six
 302 patterns of acoustic reflectivity (acoustic facies) were identified on the side-scan sonar
 303 imagery (Figure 11). The characteristic features of the six acoustic facies are detailed
 304 in Table 2. Facies 1 corresponds to rocky areas in Figure 10. Facies 2 to 6 occur in
 305 areas with little relief.

306 **4.2.1. Facies 1**

307 Figure 11 shows the distribution of Facies 1, which coincides with known reefs plotted on
 308 official nautical charts (SA Navy Nautical Chart 1017 and British Admiralty Nautical
 309 Chart 1922). The lineaments seen in Facies 1 follow several directions, but the best-
 310 defined lineaments trend WNW-ESE, parallel to the principal joint direction in the
 311 granite outcrops onshore (Boocock, 1951; Theron, 1984). Large, well-jointed, rounded
 312 granite boulders (as tall as 5m), resting on a larger rounded rocky base (massif) or
 313 protruding above the sediment, were observed by divers at Rambler Rock and near
 314 Roman Rock. The outcrops provide a solid substrate for both calcareous and soft-bodied
 315 marine organisms and are surrounded by bioclastic debris.

316 **4.2.2. Facies 2**

317 Facies 2 occurs adjacent to, or immediately north of, Facies 1, between 20m and 35m
 318 water depth (Figure 11). A diver inspection near Roman Rock revealed that Facies
 319 2 consisted of large-scale sedimentary bedforms. The bedforms, spaced 0.8m to 1.2m
 320 apart and 0.2m to 0.3m high, were symmetrical with long and straight crests that
 321 were sometimes bifurcated in a crest-parallel direction (Figure ??). The crests had
 322 the same ENE-WSW orientation as the light and dark bands on the side-scan sonar
 323 imagery. The 0.8m to 1.2m bedform wavelength is near the 0.25m (across-track) and
 324 the 2.09m (along-track) resolution limits of the side-scan sonar system and thus not

Table 2.

Facies	Relief	Acoustic Reflectivity	Sonograph Pattern	Sediment Texture	SCUBA Diver Observations	Interpretation
1	Rugged	Strong	Lineaments within an irregular blocky pattern of light and granite outcrops west of the study area. dark tones.	—	Granite outcrop, similar to the coastal granite outcrops west of the study area. Outcrops are covered with marine organisms. The base of the outcrops is surrounded by bioclastic debris.	Cape Peninsula Granite.
2	Low	Moderate	Alternating bands of light and dark tones oriented ENE-WSW and space about one meter apart.	Sand, gravelly sand, and gravel	Straight-crested bifurcating ripples with a wavelength between 0.8m to 1.2m and amplitude between 0.2m and 0.3m, ENE-WSW crest orientation.	Large-scale, long-crested trochoidal wave ripples.
3	None	Moderate to weak	Uneven featureless medium-gray tone	Sand and gravelly sand	Small (1 to 2 meter wide) patches of gravelly calcareous sediment overlying relict quartzose fine to medium sand. Ophiuroids and crinoids are common.	Patchy veneer of calcareous gravelly sediment overlying a quartzose fine to medium sand.
4	None	Weak	“Cloud-like” and “tongue-like” patches of light tone	Sand	Rippled fine to medium sand-patches. Ripples are straight-crested, symmetrical, and bifurcate. Ripples have a wavelength between 10cm and 20cm and an amplitude of 1cm to 3cm. ENE-WSW crest-orientation. Apart from some pinnid bivalves, the patches are barren.	Blanket of quartzose fine to medium sand.
5	None	Weak	Slightly speckled, featureless light tone	Sand	Rippled quartzose fine to medium sand. Ripples are straight-crested, symmetrical, and bifurcate. Ripples have a wavelength between 10cm and 20cm and amplitude ranging from 1cm to 3cm. ENE-WSW crest-orientation. Few ophiuroids and asteroids are present.	Windows of quartzose fine to medium sand.
6	None	Moderate	Patches of medium-gray tone	Sand	None.	Coarse sediment patches?

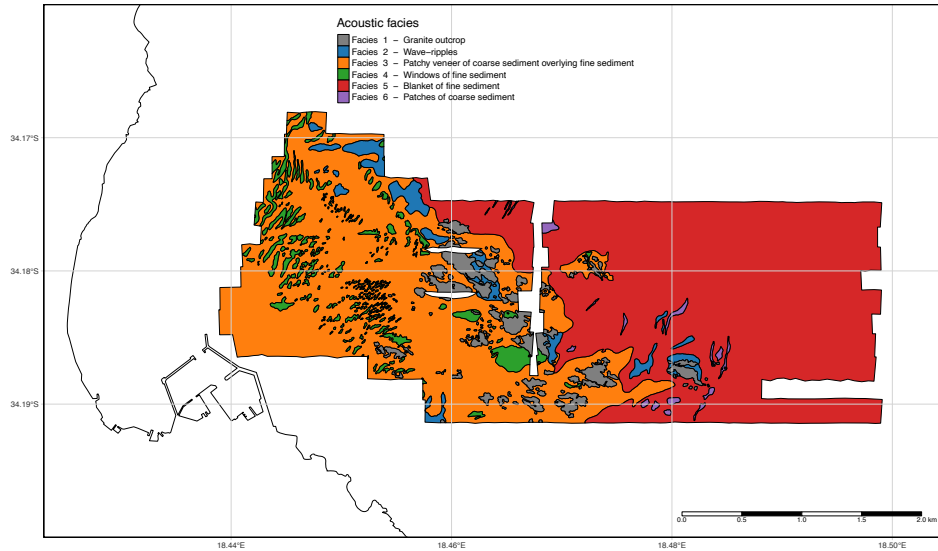


Figure 11.: Acoustic facies map of the study area

325 easy to distinguish on the side-scan sonar imagery. The bed forms were developed in
 326 calcareous gravel and sand with coarser sediment in the troughs and finer sediment on
 327 the crests.

328 4.2.3. Facies 3

329 Facies 3 occurs in the western half of the study area, at depths between 20m and 35m
 330 (Figure 11). Sediment samples from Facies 3 range from quartzose sand to calcareous
 331 gravel. The samples nearest the granite pinnacles are usually composed of shell debris
 332 such as cirripede (barnacle) and mollusc fragments, whereas the samples farther away
 333 from the rock pinnacles, between Roman Rock and the Simon's Town harbor wall,
 334 are composed of a mixture of coralline-algal fragments and quartzose sand. Dive sites
 335 C, E, F, and H (Figure 8) revealed both living and dead unattached coralline algae
 336 (subfamily Melobesioideae) forming autochthonous structures, referred to as 'maerls' or
 337 'marls' (e.g Bosence, 1976; Steneck, 1986), which create a complex habitat supporting
 338 diverse taxa (Steller, Riosmena-Rodriguez, Foster and Roberts, 2003). These maerl
 339 structures, a few meters across and centimeters high, often appear as elongated strips
 340 oriented ENE-WSW over quartzose sand and are associated with crinoids and brittle
 341 stars. Additionally, divers observed pebble-sized quartz and feldspar fragments and
 342 *Venus verrucosa* shell fragments on the seafloor in Facies 3.

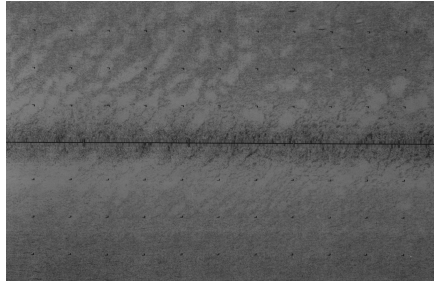
343 4.3. Sedimentology

344 4.3.1. Sediment texture

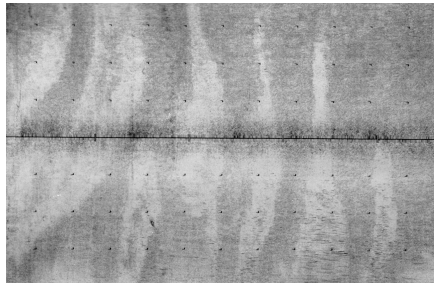
345 Figure 14 shows that the sediment samples collected in this study are either gravelly
 346 sands or sandy gravels. The samples are essentially mud-free. Figure 15 presents a
 347 breakdown of sediment texture by Acoustic Facies. Facies 3 exhibits the most variation
 348 in sediment texture, ranging from slightly gravelly sand to gravel. Most of the samples



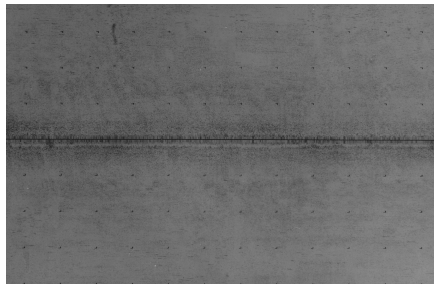
(a) Facies 1 – Cape Peninsula Granite and Facies 2 – Wave ripples



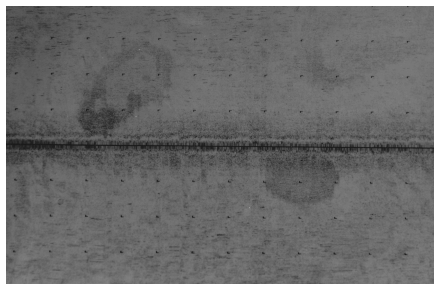
(b) Facies 4 – Cloud-like patches of fine to medium sand.



(c) Facies 4 – Tongue-like patches of fine to medium sand.

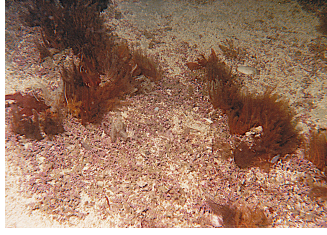


(d) Facies 4 – Cloud-like patches of fine to medium sand.



(e) Facies 6 – Coarse sediment patches within Facies 5?

Figure 12.: Example sonograms. Internal tick-marks are at 25m intervals.



(a) Unattached branching coralline algae (maerl) together with dark-coloured feather stars (*Comanthus wahlbergi*) at Dive Site F (Facies 3). The field of view is approximately one metre.



(b) Isolated granite boulder in the middle of a wave-ripple field at Dive Site D (Facies 2).



(c) Fine to medium quartzose sand in Facies 4 cloud-like pattern at Dive Site H.



(d) Small-scale ripples in fine to medium quartzose sand at Dive Site J (Facies 5). Note the ophiuroids (brittle stars) in the foreground.



(e) Rippled quartzose fine to medium sand in cloud-like patches at Dive Site H (Facies 4). The measuring staff is marked at 1cm and 10cm intervals. Note the slightly coarser material in the troughs.

Figure 13.: Underwater photographs from in-situ diver inspections. Refer to Figure 8 for dive site locations.

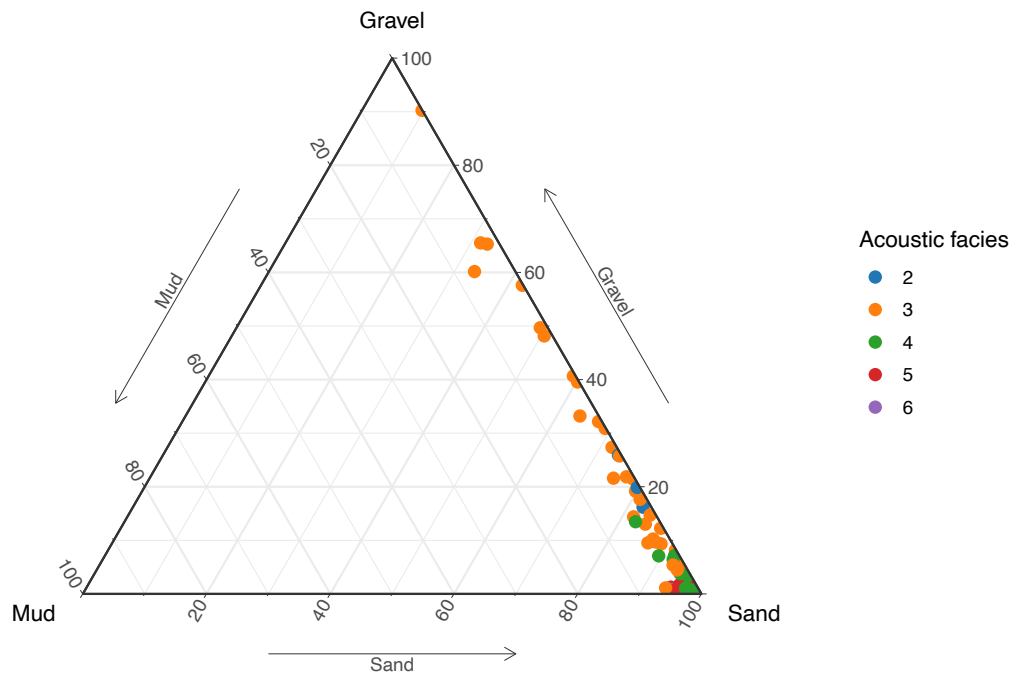


Figure 14.: Gravel-Sand-Mud ternary diagram. The sediment is largely mud-free. Samples collected in Facies 3 range from gravelly sand to gravel. Most of the samples from the other acoustic facies are slightly gravelly to gravelly sands.

349 from the other acoustic facies are slightly gravelly to gravelly sands. Figure 16 shows a
 350 clear relationship between sediment texture and sediment composition: the higher the
 351 gravel fraction, the more calcareous the sediment is. The following section presents the
 352 analysis of sediment composition, which clearly shows that the gravel fraction consists
 353 primarily of bioclastic components.

354 4.3.2. Sediment composition

355 Results from the visual examination of gravel components and binocular examination
 356 of sand components are presented in Figures 22 and 23, respectively. These show the
 357 abundance of each component for all the samples from each facies. Abundances are
 358 expressed in terms of Ingram (1965) categories. Mollusc and coralline algal fragments
 359 dominate the gravel fraction in all the sediment samples.

360 5. Interpretation

361 This section interprets the geological significance of the side-scan sonar, echosounder,
 362 sediment sample data and diver observations.

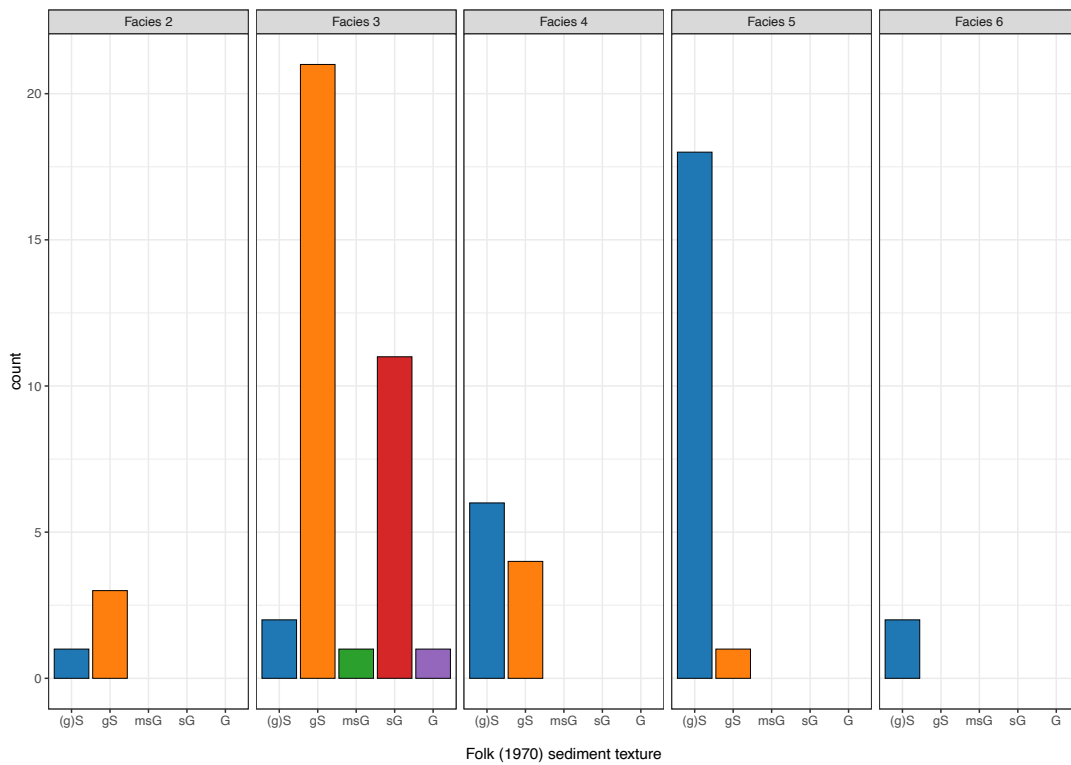


Figure 15.: Breakdown of sediment texture per facies.
 (g)S = slightly gravelly Sand, gS = gravelly Sand, msG = muddy sandy Gravel, sG = sandy Gravel, G = Gravel.

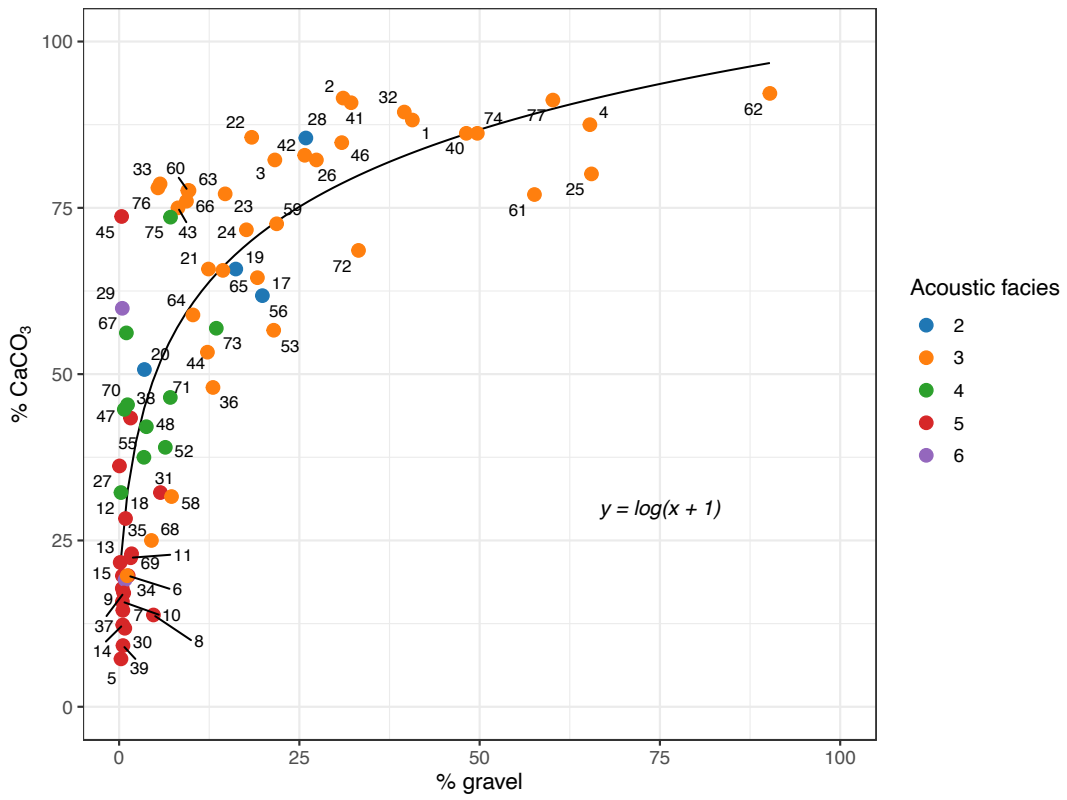


Figure 16.: Percent gravel versus percent CaCO₃. The calcareous fraction increases exponentially with an increasing gravel fraction.

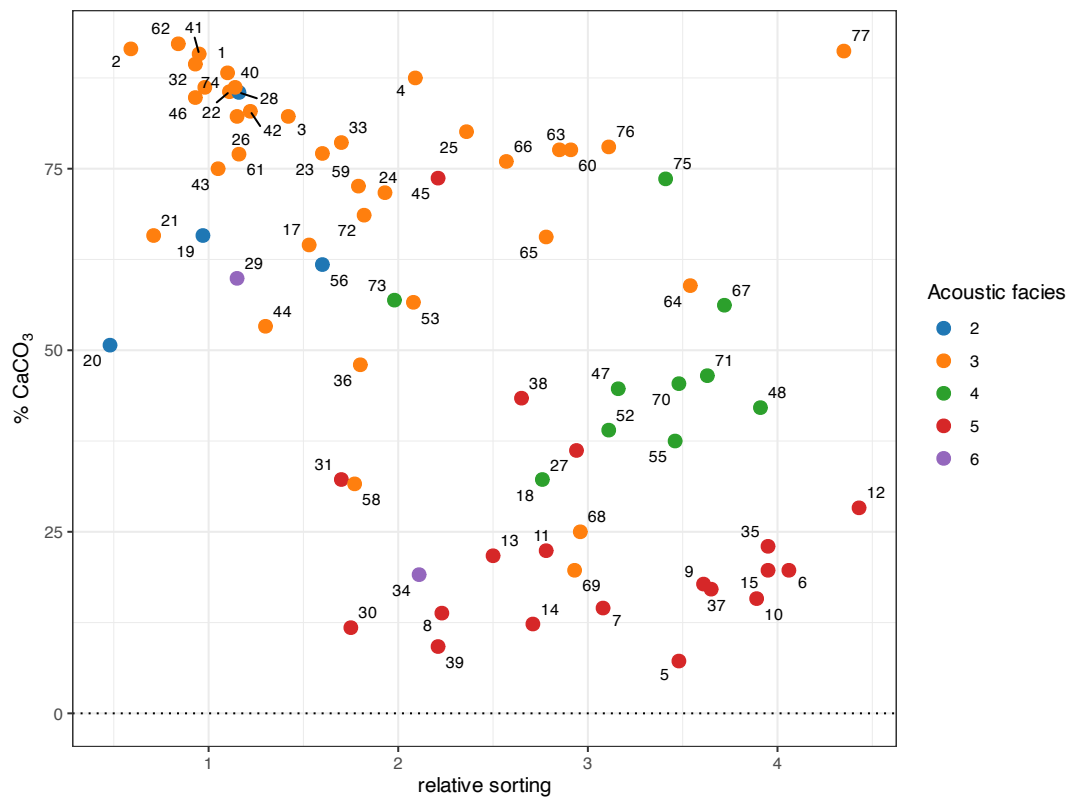


Figure 17.: Relative sorting versus CaCO₃. Facies 3 calcareous sands are better sorted than Facies 5 quartzose sands.

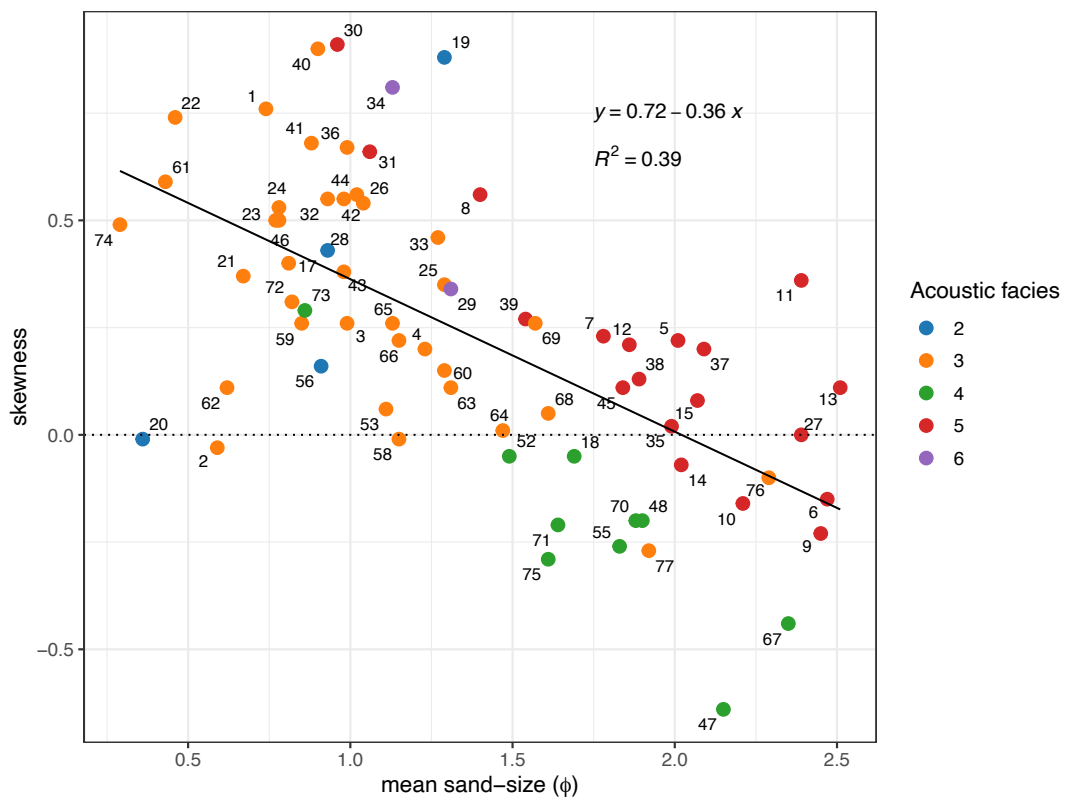


Figure 18.: Mean sand-size versus skewness. Sand becomes less positively skewed as it becomes finer-grained.

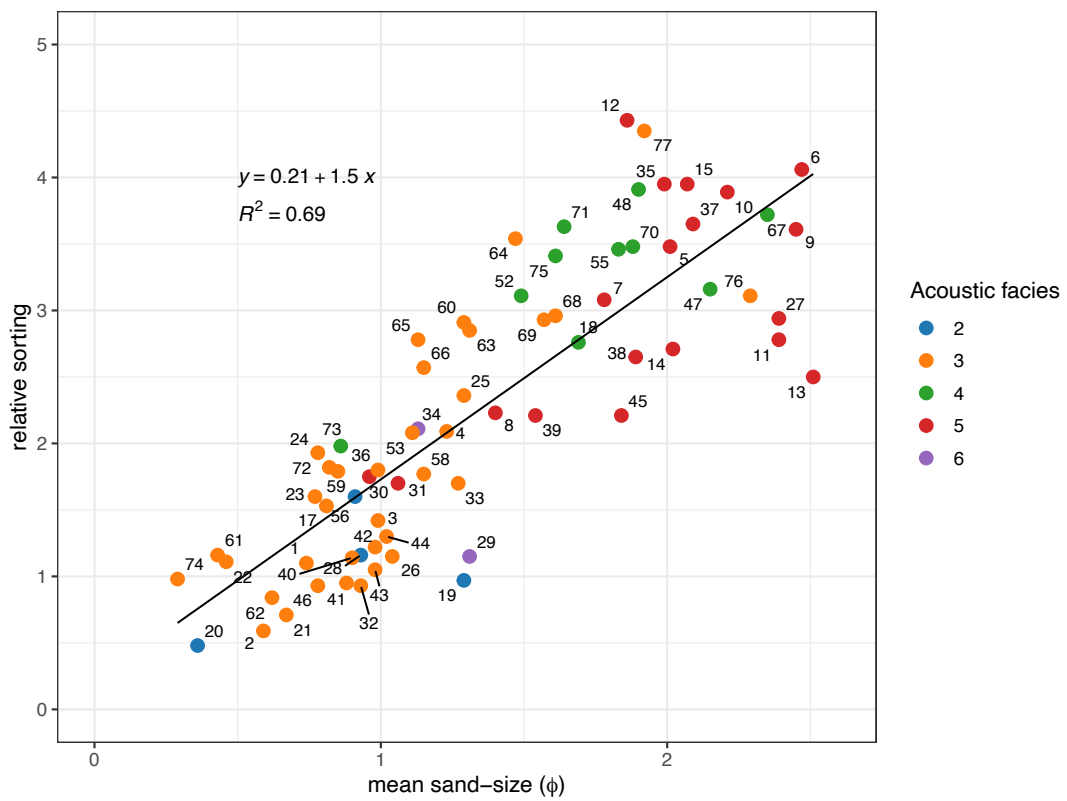


Figure 19.: Mean sand-size versus relative sand-sorting. Sand becomes less well-sorted as it becomes finer-grained.

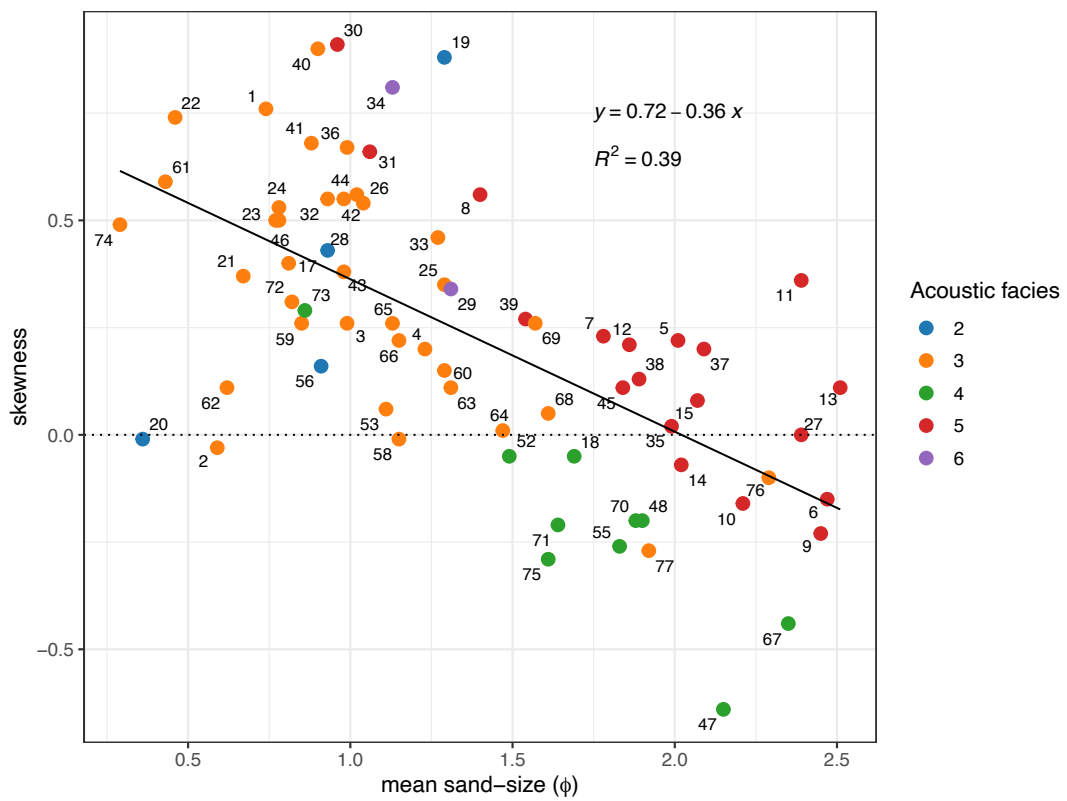


Figure 20.: Mean sand-size versus skewness. Sand becomes less positively skewed as it becomes finer-grained.

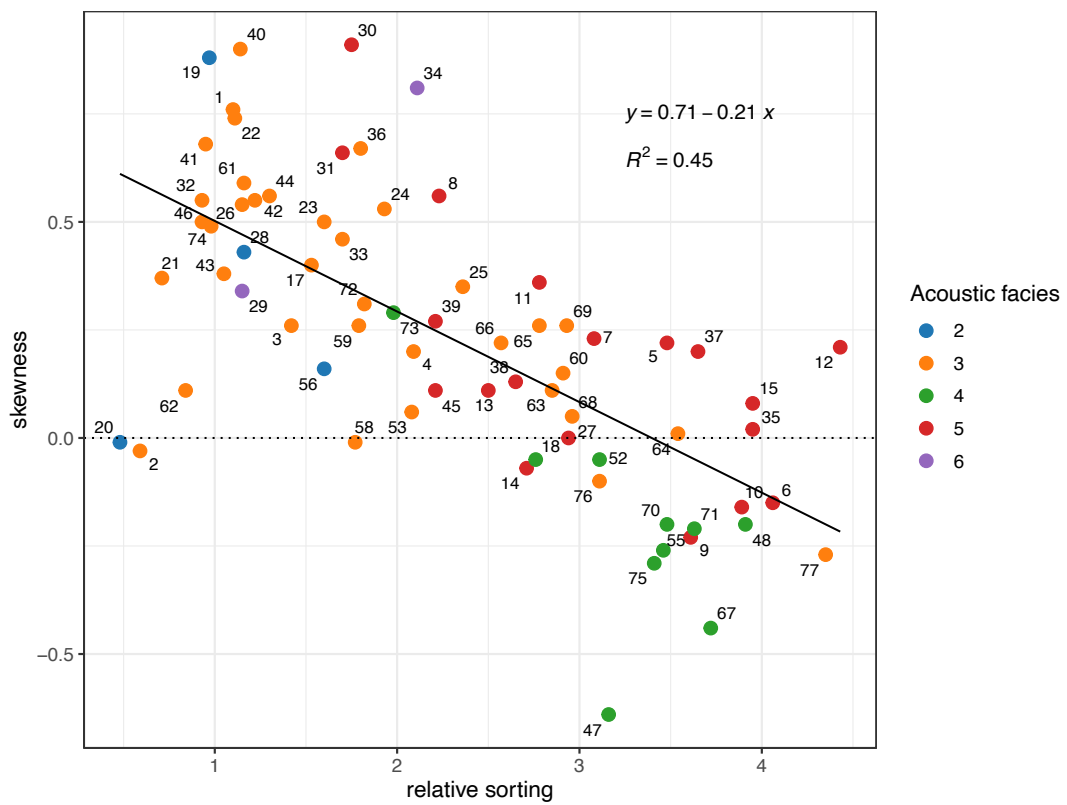


Figure 21.: Relative sorting versus skewness. Sands become more positively skewed as they become more well-sorted.

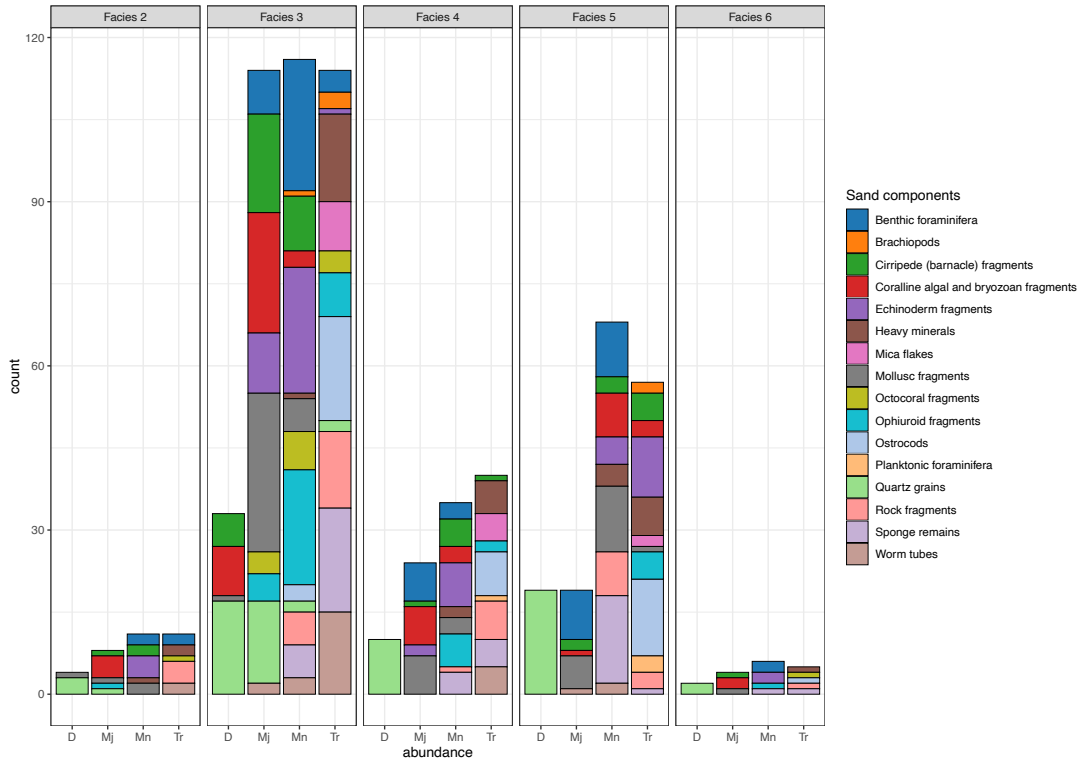


Figure 22.: Breakdown of sand components.

D = Dominant (> 50%), Mj = Major (5% - 50%), Mn = Minor (1% - 5%), Tr = Trace (< 1%)

363 **5.1. Facies 1 - Cape Peninsula Granite**

364 The pattern of reflectivity produced by the exposed Cape Peninsula Granite (Facies 1)
 365 has been observed elsewhere in False Bay and further afield in Table Bay (MacHutchon,
 366 de Beer, Van Zyl and Cawthra, 2020; Woodborne and Flemming, 2021) and Saldhana
 367 Bay (De La Cruz, 1978) and is typical of granite. The WNW-ESE lineaments seen
 368 on the side-scan sonar imagery collected in this study correspond to the principal
 369 joint direction in the Cape Peninsula Granite observed along the Simon's Town coast
 370 (Boocock, 1951; Theron, 1984). The granite outcrops observed in the side-scan sonar
 371 imagery may be described as submerged tors where the joints in the granite are more
 372 widely spaced (Du Plessis and Glass, 1991; Glass, 1977; Linton, 1955).

373 **5.2. Facies 2 - Wave Ripples**

374 The underwater photographs at dive site D (Figure 8) verify that Facies 2 represents
 375 rippled calcareous gravelly sand or sand. This pattern of reflectivity has been ob-
 376 served elsewhere along the South African coast, for example, in Saldhana Bay and off
 377 Namaqualand (De La Cruz, 1978; Flemming, 2019).

378 The symmetry, WSW-ESE orientation, and crest length of the ripples suggest that
 379 orbital currents generated by SSE swells form them and, therefore, should be more
 380 accurately defined as long-crested trochoidal wave—ripples (Reineck and Singh, 1980).
 381 The wave ripples are located near or to the north of granite reefs. This implies that
 382 the orbital currents forming these ripples are intensified when waves from the SSE

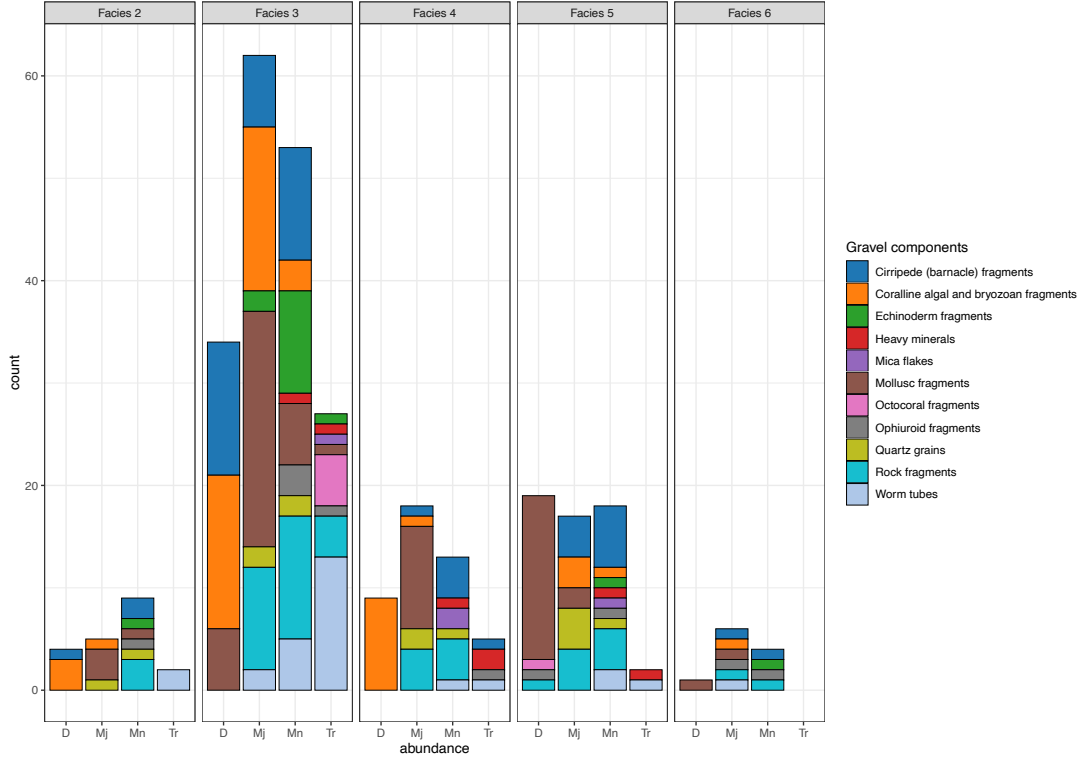


Figure 23.: Breakdown of gravel components.

D = Dominant (> 50%), Mj = Major (5% - 50%), Mn = Minor (1% - 5%), Tr = Trace (< 1%)

383 pass northwestwards over reefs. The shallow seafloor depression observed to the NW of
 384 Roman Rock (see Figure 10 – bathymetry map) is likely to have been generated by
 385 stronger bottom currents. The sediment where the wave ripples occur has a mean size
 386 of 0.56mm (coarse sand). Figure 24 suggests that the minimum orbital current velocity
 387 (μ_m) needed to move sediment of this size is approximately 0.25 to 0.3 ms^{-1} .

388 Substituting an arbitrary wave-period of 10s (within the 8s to 14s range described
 389 by Shipley (1964)), a value for u_m of 0.3 ms^{-1} and a depth (h) of either 20m or 35m
 390 (the depth—range of the wave ripples) into equation 1 (Komar and Miller, 1973), the
 391 minimum wave-heights (H) needed for wave ripple formation are 0.9m and 1.8m at
 392 depths of 20m and 35m, respectively.

$$\mu_m = \frac{\pi H}{T \sinh(2\pi h/L)} \quad (1)$$

393 where μ_m is the threshold orbital velocity (ms^{-1}), H is the wave-height (m), T is the
 394 wave period (s), L is the derived wave-length (m) where $L = 1.56T^2$, h is the water
 395 depth (m).

396 Note that Komar and Miller’s 1973 equation is based on empirical studies addressing
 397 the entrainment of spherical quartz grains. Irregularly shaped bioclastic components
 398 most likely require higher orbital velocities (i.e. higher wave heights) to move (Li, Yu,
 399 Gao and Flemming, 2020).

400 The wave ripples were inactive when inspected by divers during fair-weather condi-

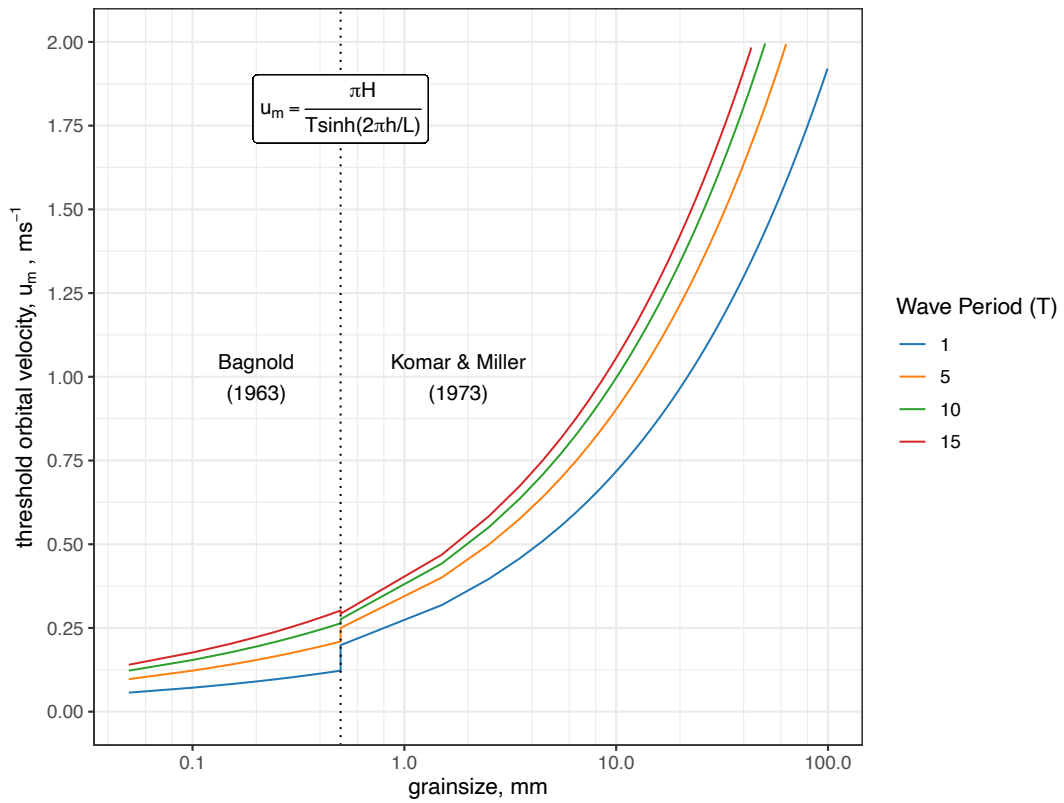


Figure 24.: Near-bottom orbital velocity u_m for sediment threshold under waves. Plot generated using computational routines described in Komar and Miller (1975). For sediment grain sizes $\leq 0.5\text{mm}$, the curves are based on Bagnold (1963) empirical data. For grain sizes $> 0.5\text{mm}$, the curves are based on Komar and Miller (1973) empirical data.

401 tions. This, together with the 0.9m to 1.8m range of minimum wave heights required
402 to generate μ_m and the quiet-water epifaunal assemblage found in the study area,
403 suggests that wave ripple formation is likely to only occur during prolonged summer
404 southeasterly gales when the highest waves occur in False Bay (Theron and Schoonees,
405 2007).

406 ***5.3. Facies 3 - Patchy Veneer of Calcareous Sediment***

407 Facies 3 represents a patchy veneer of calcareous gravel or gravelly sand overlying fine
408 to medium quartzose sand. The patchiness of the calcareous sediment is attributed to
409 many environmental factors, such as the nature of bottom—currents, type of substrate,
410 predation, and food—supply, that affect the distribution of CaCO_3 secreting organisms.
411 Maerl is present in almost every coastal ecosystem around the world (Foster, 2001).
412 It comprises broken fragments from larger fructose forms of coralline algae growing
413 on rocks. The fragments continue to grow unattached on the seafloor after they have
414 broken off (Johansen, 2018; Woelkerling, Irvine and Harvey, 1993). The concentration
415 of detritus-feeding ophiuroids on top of the maerl may be because some entrained
416 detritus becomes trapped in the interlocking branches of coralline algae as the water
417 filters through them.

418 ***5.4. Facies 4 - Windows of Calcareous Fine to Medium Sand***

419 The reflective pattern distinguishing Facies 4 from Facies 3 is produced by large patches
420 of rippled, calcareous, fine to medium quartzose sand. Facies 4 appears to represent
421 gaps in the veneer of calcareous gravelly sediment, large enough for side—scan sonar
422 to detect the underlying fine to medium quartzose sand. In contrast, in Facies 3, the
423 much smaller windows of fine to medium quartzose sand in the veneer of calcareous
424 sediment are too small to be resolved by side—scan sonar. This interpretation is based
425 on evidence provided by underwater photographs taken by divers at dive sites G and
426 H (Figures 8 and 13).

427 The WSW-ENE orientation of the “cloud-like” sand patches may be due to winnowing
428 by orbital currents generated by SSE waves, whereas the “tongue-like” patches are
429 possibly produced by a predominant northward-moving bottom-current (Atkins, 1970*b*;
430 Vos et al., 2021). The WSW-ENE crest orientation and bifurcated ripples seen by
431 divers within Facies 4 at dive sites F and H (Figures 8 and 13) suggest that these are
432 also a product of SSE-wave-generated orbital currents.

433 ***5.5. Facies 5 - Blanket of slightly calcareous fine to medium sand***

434 Facies 5 is produced by an extensive blanket of slightly calcareous, fine to medium
435 quartzose sand. The speckled areas seen on the sonographs in Facies 5 (Figure 12) are
436 attributed to small wave ripples and epifauna that cannot be resolved by side-scan
437 sonar. This interpretation is verified by underwater photographs of small-scale ripples
438 and epifauna taken at dive site J (Figure 8 and ??) and by the homogeneity of the
439 Facies 5 sediment samples. Bouma and Rapoport (1984) also found that a feature-less,
440 even-toned seafloor may be covered with features too small or of insufficient density to
441 be resolved by side-scan sonar. Consequently, they stress the importance of underwater
442 photography in verifying the interpretation of side-scan sonar imagery. This project
443 confirms the value of this approach, particularly regarding Facies 3 to 5.

444 The WSW-ENE crest orientation and bifurcation of the small-scale ripples seen in
445 Facies 5 at dive site J imply that SSE wave—generated orbital currents produce these.

446 **5.6. *Facies 6 - Coarse sediment patches***

447 Any interpretation of Facies 6 is hampered by the lack of underwater photographs,
448 diver—observations, and sufficient sediment samples. The two sediment samples from
449 Facies 6, a medium quartzose sand and a medium calcareous sand, suggest that Facies
450 6 represents medium sand. The rounded Facies 6 patches depicted in Figure 12 may
451 represent exposed saprolite.

452 **5.7. *Modern subtidal energy regime***

453 Data from the ADCP deployed off Miller’s Point, and the output of circulation models
454 show that bottom currents in the study area are generally weak, seldom exceeding
455 0.2ms^{-1} (Coleman et al., 2021). The observed epifaunal assemblage confirms that
456 the study area is a low-energy environment. The delicate filter-feeding pinnid bivalve
457 *Atrina squamifera* observed in Facies 4 typically occurs in fine sediment in a sheltered
458 environment where it is least susceptible to breakage or burial (Day, 1969, p. 143)
459 (Kilburn and Rippey, 1982, p. 167). The same applies to the delicately-branched,
460 free-living coralline—algae (maerl) which must live above the sediment in a quiet
461 environment to survive (Steneck, 1986). The precarious attachment of the detritus-
462 feeding crinoid, *Comanthus wahlbergi*, to the loose maerl and the vertically semi-
463 embedded pinnid bivalves, indicates that bottom currents must be weak. The density of
464 ophiuroids observed in Facies 3 is also indicative of a low-energy environment, according
465 to Branch and Branch (1981, p. 238) who comment: “brittle stars are often gregarious
466 and in deeper, calmer, waters dense assemblages may be found”.

467 Another indication that the subtidal zone is a low-energy environment is from a
468 side-scan sonar survey conducted three years earlier of an area overlapping the present
469 study area (Russell-Cargill, 1983). A comparison of the side-scan sonar imagery from the
470 previous survey and the present study shows no noticeable difference in the distribution
471 of the different patterns of acoustic reflectivity. Thus, the modern subtidal zone in
472 the study area is generally a stable low-energy environment, except during prolonged
473 southeasterly gales in summer, when high-energy conditions sufficient for Facies 2
474 wave-ripple formation prevail. The subtle seafloor depression observed northwest of
475 Roman Rock (Figure 10) is likely the result of wave-driven orbital currents scouring
476 the seabed.

477 **5.8. *Sediment mixing***

478 Flemming (1982) asserts that the sediment distribution in False Bay can be explained
479 in terms of the sediment-mixing model of Folk and Ward (1957). He states: “the mixing
480 process between two hydraulic populations of different mean sizes follows a predictable
481 pattern revealed in the appropriate scatter plots. Progressive mixing implies that a
482 well-sorted coarse population will initially become increasingly finer, more positively
483 skewed and less well-sorted as the proportion of fine sediment increases. By analogy, a
484 well-sorted fine population will become increasingly coarser, more negatively skewed
485 and less well—sorted the greater the proportion of coarse sediment.” (Flemming, 1982,
486 p. 15).

487 Plotting the percent $CaCO_3$ against relative sand-sorting, one sees that the quartzose
488 sands from Facies 4 and 5 are not as well-sorted as the calcareous sediment from Facies
489 2 and 3 (Figure 17). Figures 19 to 21 (where mean sand size, relative sand-sorting and
490 skewness are plotted against each other) show that the coarse relatively well-sorted sand
491 in Facies 3 becomes less well-sorted and more positively skewed as the proportion of fine
492 sand increases. This trend conforms to the Folk and Ward (1957) sediment—mixing
493 model. Mixing is most apparent in Facies 3 because it has diverse end members, one a
494 calcareous gravel and the other a moderately- to well—sorted fine to medium quartzose
495 sand, whereas the other facies are predominantly coarse calcareous sediment or a fine
496 to medium quartzose sand.

497 The degree of mixing depends on the intensity of bottom—current activity and the
498 extent of bioturbation. The mixing of sediments in Facies 3 probably occurs because
499 the underlying exposed fine to medium quartzose sand is more easily entrained than
500 the overlying patchy veneer of coarse calcareous sediment. Once the bottom current
501 velocity decreases to a point where suspension is no longer possible, the fine to medium
502 quartzose sand settles out on the calcareous sand and gravel. In this way, the mixing
503 process depicted in Figures 19 to 20 is thought to occur.

504 *5.9. Quaternary sedimentation*

505 This section discusses the Quaternary sedimentary history of the study area, gleaned
506 from literature on sea-level fluctuations and the probable relationship between the six
507 sonograph facies.

508 During the last glacial maximum (between 26.5 and 19 ka), sea level dropped as much
509 as 130m below its present elevation (Clark, Dyke, Shakun, Carlson, Clark, Wohlfarth,
510 Mitrovica, Hostetler and McCabe, 2009; Compton, Mulabisana and McMillan, 2002;
511 Cooper, Green and Compton, 2018; Yokoyama, Lambeck, De Deckker, Johnston and
512 Fifield, 2000). The Cape Flats would then have extended beyond the present-day
513 entrance to False Bay. Apart from the granite pinnacles, the study area would have
514 formed part of an extensive dune field deposited on the newly exposed floor of False
515 Bay (Bowie, 1966). Parts of the area would probably also be covered by sandstone
516 debris (talus) deposited by mass wasting along the steep flanks of the Swartberg
517 mountain (Rogers, 2018). During the subsequent Flandrian transgression, these Late
518 Pleistocene sediments were probably eroded and redistributed by wave action as the
519 sea transgressed across the study area.

520 This process persists today at Swartklip on the northern shore of False Bay. Here, a
521 50m thick succession of Late Pleistocene sands is being eroded and redistributed by
522 wave action (Flemming, 1982). Barwis and Tankard (1983) recognise four depositional
523 facies in the Swartklip succession. From the base up, these are beach, estuarine,
524 washover—fan, and aeolian facies (i.e. a Late Pleistocene regressive sequence). The
525 aeolian sediment seen at Swartklip and in boreholes north of Swartklip, consists of
526 cross-bedded, slightly calcareous, moderately- to well-sorted fine to medium quartzose
527 sand (Hay, 1981). As the quartzose sand found in the study area has textural properties
528 similar to those found at Swartklip, it is concluded that it is also derived from aeolian
529 deposits that were reworked by waves during the Flandrian transgression. In other
530 words, the quartzose sand found in the study area is a relict of both an aeolian and a
531 shoreline environment, but presently lies in a modern low-energy subtidal environment
532 episodically affected by southeasterly gales in summer. Therefore, it is not only “relict”
533 but also “palimpsest” (McManus, 1975). Palimpsest sediment has the petrographic

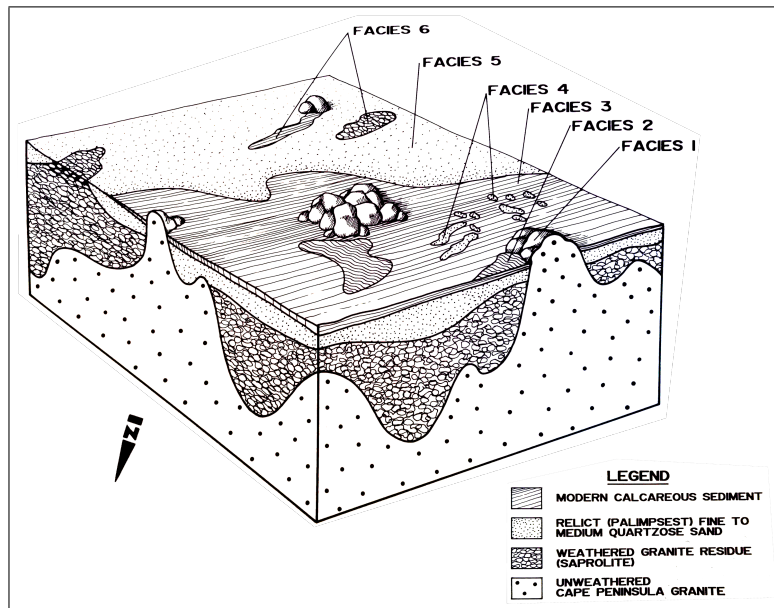


Figure 25.: Sketch showing the probable geological relationship between the six acoustic facies.

534 attributes of an earlier and later (in this instance, modern) sedimentary environment
 535 (Swift, Stanley and Curray, 1971).

536 Towards the end of the Flandrian transgression, the study area would have be-
 537 come fully submerged, marking the onset of the modern sedimentary environment in
 538 which calcareous sediment derived from molluscs, cirripedes, coralline algae, and other
 539 carbonate-secreting marine organisms, started to accumulate on top of the palimpsest
 540 quartzose sand (Martins and Barboza, 2005). Figure 25 shows how the six acoustic
 541 facies are thought to relate to one another.

542 6. Summary and conclusions

543 Our side-scan sonar survey of a 12km² area in the northwestern corner of False Bay
 544 revealed six distinct acoustic facies, interpreted using echosounder data, bottom
 545 samples, and SCUBA diver observations.

546
 547 Facies 1 shows Cape Peninsula Granite outcrops, matching onshore patterns,
 548 with lineaments reflecting the principal WNW-ESE joint direction.

549
 550 Facies 2 is marked by stationary, long-crested, trochoidal wave ripples, likely formed
 551 by currents from southeasterly gales.

552
 553 Facies 3 features an uneven grey tone of calcareous gravelly sand derived from marine
 554 organisms in the shallower western areas.

555
 556 Facies 4 appears as 'cloud-like' and 'tongue-like' light patches, indicating win-
 557 dows of underlying rippled quartzose sand.

558

559 Facies 5 is a light-toned blanket of rippled quartzose sand in deeper eastern
560 regions.

561

562 Facies 6 consists of medium-grey patches within Facies 5, possibly represent-
563 ing coarse sediment, pending further confirmation.

564

565 Circulation models and epifaunal assemblages suggest the study area is a low-
566 energy subtidal environment. Sediment analysis indicates mixing between calcareous
567 and quartzose sediments, particularly in Facies 3. The quartzose sand is likely reworked
568 from Late Pleistocene deposits, making the subtidal sands “relict” and “palimpsest”.
569 The deposition of calcareous sediment over this palimpsest sand marks the onset of
570 the modern subtidal environment.

571 This study demonstrates the complexity of the seafloor geology off Simon’s Town,
572 underscoring the value of bottom sampling, diver observations, and underwater pho-
573 tography in validating sonar imagery. It also highlights the need for future research to
574 explore sediment dynamics further, especially considering grain composition, shape, and
575 size and their impact on sediment movement. More comprehensive bottom-current and
576 wave data, along with advanced hydrodynamic models, are necessary for a quantitative
577 analysis of sediment movement.

578 **CRedit authorship contribution statement**

579 Andrew Terhorst: Conceptualization, Formal analysis, Investigation, Methodology,
580 Project administration, Writing – original draft. John Rogers: Supervision, Writing –
581 review & editing.

582 **Declaration of competing interest**

583 The authors declare that they have no known competing financial interests or personal
584 relationships that could have appeared to influence the work reported in this paper.

585 **Data availability**

586 Interested readers can access the spatial and sedimentological data used in this
587 study via the “Mendeley Data” open data repository at <https://data.mendeley.com/datasets/r6995krm6v/1>.

589 **Acknowledgments**

590 The original study was sponsored by the South African Navy (IMT projects MT-073
591 and OH-004) and by an M.Sc study grant from the South African Foundation for
592 Research Development (FRD). This updated study received support from Australia’s
593 Commonwealth Scientific and Industrial Research Organisation (CSIRO). The authors
594 would like to express their gratitude to Professor Burghard Flemming, Dr. Christo
595 Rautenbach, Dr. Marc de Vos, Mr. Carl Wainman, the late Mr. Ewald Teichert, Mr.
596 Ethan Potgieter, Mr. Bill Russell-Cargill, and Mr. Michael MacHutchon for their

597 valuable guidance and input. Special thanks are due to the scientific divers from the
598 Institute for Maritime Technology and the University of Cape Town, whose critical
599 role in ground-truthing the side-scan sonar imagery was indispensable. Finally, we
600 commend Mr. Barry Petersen, the skipper of the vessels “Shirley-T” and “Annie-K”,
601 for his exceptional seamanship.

602 References

- 603 Atkins, G. (1970a), ‘Thermal structure and salinity of False Bay’, *Transactions of the Royal*
604 *Society of South Africa* **39**(2), 117–128.
- 605 Atkins, G. (1970b), ‘Winds and current patterns in False Bay’, *Transactions of the Royal*
606 *Society of South Africa* **39**(2), 139–148.
- 607 Backeberg, N., Reid, D., Trumbull, R. and Romer, R. (2011), ‘Petrogenesis of the False Bay
608 Dyke Swarm, Cape Peninsula, South Africa: evidence for basement assimilation’, *South*
609 *African Journal of Geology* **114**(3-4), 335–352.
- 610 Bagnold, R. (1963), *Mechanics of marine sedimentation*, Vol. 3, Interscience, New York, N.Y.,
611 pp. 507–528.
- 612 Barwis, J. H. and Tankard, A. J. (1983), ‘Pleistocene shoreline deposition and sea-level history
613 at Swartklip, South Africa’, *Journal of Sedimentary Research* **53**(4), 1281–1294.
- 614 Belcher, R. W. and Kisters, A. F. (2003), ‘Lithostratigraphic correlations in the western branch
615 of the Pan-African Saldania belt, South Africa: the Malmesbury Group revisited.’, *South*
616 *African Journal of Geology* **106**(4), 327–342.
- 617 Birch, G. (1981), ‘The karbonat-bombe: a precise, rapid and cheap instrument for determining
618 calcium carbonate in sediments and rocks’, *South African Journal of Geology* **84**(3), 199–203.
- 619 Boocock, C. (1951), ‘The structural features and inclusions of the Cape Peninsula granite’,
620 *Transactions of the Royal Society of South Africa* **33**(2), 243–276.
- 621 Bosence, D. (1976), ‘Ecological studies on two unattached coralline algae from western Ireland.’,
622 *Palaeontology* **19**(2), 365–395.
- 623 Bouma, A. and Rapoport, M. (1984), ‘Verification of side-scan sonar acoustic imagery by
624 underwater photography’, *Underwater Photography* pp. 279–294.
- 625 Bowie, D. (1966), The Marine Geology of False Bay, Master’s thesis, University of Cape Town.
- 626 Bowie, D., Fuller, A. and Siesser, W. (1970), ‘The marine sediments of False Bay’, *Transactions*
627 *of the Royal Society of South Africa* **39**(2), 149–161.
- 628 Branch, G. and Branch, M. (1981), *The living shores of southern Africa*, Struik Publishers.
- 629 Brink, V. and Rogers, J. (1985), Rapid granulometry of sand using a computer-linked settling-
630 tube, Bulletin 15, Joint UCT/Geological Survey Marine Geoscience Unit.
- 631 Clark, P. U., Dyke, A. S., Shakun, J. D., Carlson, A. E., Clark, J., Wohlfarth, B., Mitrovica,
632 J. X., Hostetler, S. W. and McCabe, A. M. (2009), ‘The last glacial maximum’, *science*
633 **325**(5941), 710–714.
- 634 Coleman, F., Diedericks, G., Theron, A. and Lencart e Silva, J. (2021), ‘Three-dimensional
635 modelling of the circulation in False Bay, South Africa’, *African Journal of Marine Science*
636 **43**(1), 95–118.
- 637 Compton, J. S., Mulabisana, J. and McMillan, I. (2002), ‘Origin and age of phosphorite from
638 the Last Glacial Maximum to Holocene transgressive succession off the Orange River, South
639 Africa’, *Marine Geology* **186**(3-4), 243–261.
- 640 Cooper, J., Green, A. and Compton, J. (2018), ‘Sea-level change in southern Africa since the
641 Last Glacial Maximum’, *Quaternary Science Reviews* **201**, 303–318.
- 642 Daniels, T., Fearon, G., Vilaplana, A., Hewitson, B. and Rautenbach, C. (2022), ‘On the
643 importance of wind generated waves in embayments with complex orographic features—A
644 South African case study’, *Applied Ocean Research* **128**, 103355.
- 645 Darbyshire, M. (1966), The surface waters near the coasts of southern Africa, in ‘Deep Sea
646 Research and Oceanographic Abstracts’, Vol. 13, Elsevier, pp. 57–81.

- 647 Davies, J. (1980), *Geographical Variation in Coastal Development*, Geomorphology Texts, 4th
648 edn, Longman.
- 649 Day, J. H. (1969), *A Guide to the Marine Life on South African Shores*, Balkema.
- 650 Day, R. (1986), Magnetometric mapping of the False Bay dolerites. Joint Geological Sur-
651 vey/University of Cape Town Marine Geoscience Unit, Technical report, Technical Report
652 16.
- 653 De La Cruz, M. (1978), Marine Geophysical and Geological Investigations in Saldanha Bay,
654 Technical Report 9, Joint Geological Survey/University of Cape Town Marine Geoscience
655 Group.
- 656 Du Plessis, A. and Glass, J. (1991), 'The geology of False Bay', *Transactions of the Royal*
657 *Society of South Africa* **47**, 495.
- 658 Flemming, B. (1976), 'Rocky Bank - Evidence for a relict wave-cut platform', *Annals of the*
659 *South African Museum* **71**, 33–48.
- 660 Flemming, B. (1982), The Geology of False Bay (Western Cape, South Africa) with special
661 emphasis on modern sediments, Technical Report C/SEA 8253, Csir.
- 662 Flemming, B. and Thum, A. (1978), 'The settling tube—a hydraulic method for grain size
663 analysis of sands', *Kieler Meeresforschungen Sonderheft* **4**, 82–95.
- 664 Flemming, B. W. (2019), Ripples and dunes: do flumes tell the whole story?, in 'MARID VI.
665 Sixth International Conference on Marine and River Dune Dynamics', pp. 89–94.
- 666 Folk, R. L. and Ward, W. C. (1957), 'Brazos River bar [Texas]; a study in the significance of
667 grain size parameters', *Journal of Sedimentary Research* **27**(1), 3–26.
- 668 Foster, M. S. (2001), 'Rhodoliths: between rocks and soft places', *Journal of phycology* **37**(5), 659–
669 667.
- 670 Fourie, J.-P., Ansoorge, I., Backeberg, B., Cawthra, H. C., MacHutchon, M. R. and van Zyl,
671 F. W. (2015), 'The influence of wave action on coastal erosion along monwabisi beach, cape
672 town', *South African Journal of Geomatics* **4**(2), 96–109.
- 673 Fuller, A. O. (1961), 'Size distribution characteristics of shallow marine sands from the Cape
674 of Good Hope, South Africa', *Journal of Sedimentary Research* **31**(2), 256–261.
- 675 Fuller, A. O. (1962), 'Systematic fractionation of sand in the shallow marine and beach
676 environment off the South African coast', *Journal of Sedimentary Research* **32**(3), 602–606.
- 677 Gentle, R. (1971), 'Pre-Quaternary geology of the continental shelf between Cape Infanta
678 and Cape Town', *Technical Report, South African National Commission of Oceanographic*
679 *Research, Marine Geology Programme* **3**, 13–27.
- 680 Gentle, R. (1973), 'Sidescan Sonar in Marine Geological Investigations of the South African
681 Continental Shelf', *South African Journal of Science* **69**(12), 380.
- 682 Glass, G. and Gasson, B. (1980), *Geology, morphology, sediment cover and movement*, False
683 Bay Conservation Society Cape Town, South Africa, pp. 15–25.
- 684 Glass, J. (1977), 'Deep weathering of the southwestern Cape Granite and Malmesbury Group:
685 palaeoclimatic implications', *Techn. Rep. Joint Geol. Survey/Univ. Cape Town Marine*
686 *Geosci. Group* **9**, 118–135.
- 687 Glass, J. and Du Plessis, A. (1976), The bathymetry of False Bay as an indicator of sea floor
688 geology, in 'Proc. 1st interdisciplinary Conf. mar. freshwater Res. S. Afr'.
- 689 Grundlingh, M. and Largier, J. (1991), 'Physical oceanography of False Bay: a review', *Royal*
690 *Society of South Africa. Transactions TRSAAC*, **47**(4/5).
- 691 Grundlingh, M. and Potgieter, E. (1993), 'Unique thermal record in False Bay', *South African*
692 *Journal of Science* **89**, 510–512.
- 693 Haughton, S. H. (1933), *The Geology of Cape Town and Adjoining Country...*, Geological
694 Survey.
- 695 Hay, E. R. (1981), A stratigraphic and sedimentological analysis of borehole data from a portion
696 of the cape flats. Honours Thesis.
- 697 Hersbach, H., Bell, B., Berrisford, P., Hirahara, S., Horányi, A., Muñoz-Sabater, J., Nicolas,
698 J., Peubey, C., Radu, R., Schepers, D. et al. (2020), 'The era5 global reanalysis', *Quarterly*
699 *Journal of the Royal Meteorological Society* **146**(730), 1999–2049.
- 700 Ingram, R. L. (1965), 'Facies maps based on the megascopic examination of modern sediments',

701 *Journal of Sedimentary Research* **35**(3), 619–625.

702 Johansen, H. W. (2018), *Coralline algae: a first synthesis*, CRC press.

703 Jury, M. R. (2020), ‘Coastal gradients in False Bay, south of Cape Town: what insights can be
704 gained from mesoscale reanalysis?’, *Ocean Science* **16**(6), 1545–1557.

705 Kidd, R. B., Simm, R. W. and Searle, R. C. (1985), ‘Sonar acoustic facies and sediment
706 distribution on an area of the deep ocean floor’, *Marine and Petroleum Geology* **2**(3), 210–
707 221.

708 Kilburn, R. and Rippey, E. (1982), *Sea shells of southern Africa*, Macmillan South Africa.

709 Komar, P. D. and Miller, M. C. (1973), ‘The threshold of sediment movement under oscillatory
710 water waves’, *Journal of Sedimentary Petrology* **43**(4), 1101 – 1110.

711 Komar, P. D. and Miller, M. C. (1975), ‘On the comparison between the threshold of sediment
712 motion under waves and unidirectional currents with a discussion of the practical evaluation
713 of the threshold: Reply’, *Journal of Sedimentary Research* **45**(1).

714 Li, Y., Yu, Q., Gao, S. and Flemming, B. W. (2020), ‘Settling velocity and drag coefficient of
715 platy shell fragments’, *Sedimentology* **67**(4), 2095–2110.

716 Lie, U. and Pamatmat, M. M. (1965), ‘Digging characteristics and sampling efficiency of the
717 0.1 m² Van Veen Grab’, *Limnology and Oceanography* **10**(3), 379–384.

718 Linton, D. L. (1955), ‘The problem of tors’, *The Geographical Journal* **121**(4), 470–487.

719 MacHutchon, M. (2015), ‘Geophysical monitoring of coastal erosion and cliff retreat of Monwabisi
720 Beach, False Bay, South Africa’, *South African Journal of Geomatics* **4**(2), 80–95.

721 MacHutchon, M., de Beer, C., Van Zyl, F. and Cawthra, H. (2020), ‘What the marine geology
722 of Table Bay, South Africa can inform about the western Saldania Belt, geological evolution
723 and sedimentary dynamics of the region’, *Journal of African Earth Sciences* **162**, 103699.

724 Mallory, J. (1970), ‘The bathymetry and microrelief of False Bay’, *Transactions of the Royal
725 Society of South Africa* **39**(2), 109–112.

726 Marchant, J. and Flemming, B. (1978), ‘Granite erratics in a sandstone boulder-beach in False
727 Bay-independent evidence for a marine transgression’, *Transactions of the Geological Society*
728 pp. 219–221.

729 Martins, L. and Barboza, E. (2005), ‘Sand–gravel marine deposits and grain-size properties’,
730 *Gravel* **3**, 59–70.

731 McManus, D. (1975), ‘Modern versus relict sediment on the continental shelf’, *Geological Society
732 of America Bulletin* **86**(8), 1154–1160.

733 Morgans, J. F. C. (1956), ‘The benthic ecology of False Bay, with notes on the analysis of
734 shallow-water soft substrata’.

735 Müller, G. and Gastner, M. (1971), ‘The ‘Karbonat-Bombe’, a simple device for the determination
736 of carbonate content in sediment, soils, and other materials’, *Neues Jahrbuch für Mineralogie-
737 Monatshefte* **10**, 466–469.

738 Munsell, A. (1975), *Soil Color Charts*, Macbeth Division of Kollmorgen Corporation, Baltimore,
739 MD, USA.

740 Murray, J. and Renard, A. F. (1891), *Report on deep-sea deposits based on the specimens
741 collected during the voyage of HMS Challenger in the years 1872 to 1876*, HM Stationery
742 Office.

743 Pfaff, M. C., Logston, R. C., Raemaekers, S. J., Hermes, J. C., Blamey, L. K., Cawthra, H. C.,
744 Colenbrander, D. R., Crawford, R. J., Day, E., Du Plessis, N. et al. (2019), ‘A synthesis of
745 three decades of socio-ecological change in False Bay, South Africa: setting the scene for
746 multidisciplinary research and management’, *Elementa: Science of the Anthropocene* **7**.

747 Rautenbach, C., Barnes, M. A. and de Vos, M. (2019), ‘Tidal characteristics of South Africa’,
748 *Deep Sea Research Part I: Oceanographic Research Papers* **150**, 103079.

749 Reineck, H.-E. and Singh, I. B. (1980), Current and wave ripples, in ‘Depositional Sedimentary
750 Environments’, Springer, pp. 22–55.

751 Retief, G. d. F. (1970), ‘Sediment transport in Gordon’s Bay’, *Transactions of the Royal Society
752 of South Africa* **39**(2), 163–182.

753 Rogers, J. (2018), *Geological Adventures in the Fairest Cape: Unlocking the Secrets of its
754 Scenery*, Council for Geoscience Pretoria.

- 755 Russell-Cargill, W. (1982), Project Hydra: General background to the project development,
756 Technical report Tv-019082, Institute for Maritime Technology.
- 757 Russell-Cargill, W. (1983), Project Hydra: General background to the project development.,
758 Technical Report Tv-019-82, Institute for Maritime Technology.
- 759 Salonen, N. and Rautenbach, C. (2021), ‘Toward nearshore, bathymetry induced wave amplifi-
760 cation in False Bay, South Africa’, *AIP Advances* **11**(7), 075209.
- 761 Scheepers, R. and Schoch, A. (2006), Geological Society of South Africa, chapter The Cape
762 Granite Suite, pp. 421–432.
- 763 Schoonees, J., Scholtz, D., Van Tonder, A., Moller, J. and Lenhoff, L. (1983), Valsbaai: Veldata
764 verslag, Technical Report C/sea 8219, Council for Scientific and Industrial Research.
- 765 Schulze, B. (1965), *Climate of South Africa. Part 8, General Survey*, SA Weather Bureau.
- 766 Shipley, A. (1964), ‘Some aspects of wave refraction in False Bay’, *South African Journal of*
767 *Science* **60**(4), 115–120.
- 768 Simpson, E., Du Plessis, A. and Forder, E. (1970), ‘Bathymetric and magnetic traverse
769 measurements in False Bay and west of the Cape Peninsula’, *Transactions of the Royal*
770 *Society of South Africa* **39**(2), 113–116.
- 771 Steller, D. L., Riosmena-Rodriguez, R., Foster, M. S. and Roberts, C. A. (2003), ‘Rhodolith bed
772 diversity in the Gulf of California: the importance of rhodolith structure and consequences
773 of disturbance’, *Aquatic Conservation: Marine and Freshwater Ecosystems* **13**(S1), S5–s20.
- 774 Steneck, R. S. (1986), ‘The ecology of coralline algal crusts: convergent patterns and adaptative
775 strategies’, *Annual Review of Ecology and Systematics* **17**(1), 273–303.
- 776 Stephenson, A. (2016), ‘Harmonic analysis of tides using TideHarmonics’, URL [https://CRAN.](https://CRAN.R-project.org/package=TideHarmonics)
777 [R-project. org/package= TideHarmonics](https://CRAN.R-project.org/package=TideHarmonics) .
- 778 Swift, D. J., Stanley, D. J. and Curray, J. R. (1971), ‘Relict sediments on continental shelves: a
779 reconsideration’, *The Journal of Geology* **79**(3), 322–346.
- 780 Terhorst, A. (1987), ‘The seafloor environment off Simon’s Town in False Bay revealed by
781 side-scan sonar, bottom sampling, diver observations and underwater photography’.
- 782 Theron, A. and Schoonees, J. (2007), ‘Sand transport at and shoreline response to a breakwater
783 attached to a large tidal pool at Monwabisi, Cape Town’, *Journal of the South African*
784 *Institution of Civil Engineering* **49**(2), 2–9.
- 785 Theron, J. (1984), ‘The geology of Cape Town and environs: Explanation sheets for 3318 CD
786 and DC and 3418 AB, AD and BA’, p. 77.
- 787 Van Zyl, F. (2011), Marine geophysical survey report: Table mountain marine protected area
788 phase 2 (false bay–simons town to cape point), Technical report, Council for Geoscience,
789 Bellville, Cape Town.
- 790 Vos, M. d., Vichi, M. and Rautenbach, C. (2021), ‘Simulating the Coastal Ocean Circulation
791 Near the Cape Peninsula Using a Coupled Numerical Model’, *Journal of Marine Science*
792 *and Engineering* **9**(4), 359.
- 793 Wainman, C., Polito, A. and Nelson, G. (1987), ‘Winds and subsurface currents in the False
794 Bay region, South Africa’, *South African Journal of Marine Science* **5**(1), 337–346.
- 795 Woelkerling, W. J., Irvine, L. and Harvey, A. S. (1993), ‘Growth-forms in non-geniculate
796 coralline red algae (Coralliinales, Rhodophyta)’, *Australian systematic botany* **6**(4), 277–293.
- 797 Woodborne, M. and Flemming, B. (2021), ‘Sedimentological evidence for seiching in a swell-
798 dominated headland-bay system: Table Bay, Western Cape, South Africa’, *Geo-Marine*
799 *Letters* .
- 800 Yokoyama, Y., Lambeck, K., De Deckker, P., Johnston, P. and Fifield, L. K. (2000), ‘Timing of
801 the Last Glacial Maximum from observed sea-level minima’, *Nature* **406**(6797), 713–716.